ADDIS ABABA UNIVERSITY
SCHOOL OF GRADUATE STUDIES
FACULTY OF TECHNOLOGY
ELECTRICAL AND COMPUTER ENGINEERING
DEPARTMENT

Design and Simulation of Multiband Microstrip Patch Antenna for Mobile Communications

By

Daniel Mammo

A thesis submitted to the school of Graduate studies of Addis Ababa University in partial fulfillment of the requirements for the degree of

Masters of Science

In

Electrical Engineering

Date: September 2006 G.C.

Addis Ababa, Ethiopia

ADDIS ABABA UNIVERSITY
SCHOOL OF GRADUATE STUDIES
FACULTY OF TECHNOLOGY
ELECTRICAL AND COMPUTER ENGINEERING
DEPARTMENT

Design and Simulation of Multiband Microstrip Patch Antenna for Mobile Communications

By
Daniel Mammo

Advisor

Dr - ing. Mohammed Abdo

ADDIS ABABA UNIVERSITY

SCHOOL OF GRADUATE STUDIES

Design and Simulation of Multiband Microstrip Patch Antenna for Mobile Communications

BY

Daniel Mammo

FACULTY OF TECHNOLOGY

APPROVAL BY BOARD OF EXAMINERS

_____	_____
Chairman Department of Graduate Committee	Signature
_____	_____
Advisor	Signature
_____	_____
Examiner	Signature
_____	_____
External Examiner	Signature

Declaration

I, the undersigned, declare that this thesis is my original work, has not been presented for a degree in this or any other university, and all sources of materials used for the thesis have been fully acknowledged.

Name: Daniel Mammo

Signature: _____

Place: Addis Ababa

Date of submission: _____

This thesis has been submitted for examination with my approval as a university advisor.

Dr.Ing. Mohammed Abdo _____

Advisor's Name Signature

ACKNOWLEDGMENTS

Working on the MSc thesis in the area of multiband microstrip antennas is one of the most valuable and exciting experiences in my education. The knowledge I learned and the confidence I gained during the study years will be beneficial to the whole of my life.

I am greatly indebted to my advisor, Dr.-Ing Mohammed Abdo, who takes so much patience and effort in mentoring and helping me in every aspect to complete the thesis work on time. Dr.-Ing Mohammed gave me direction in every step of my thesis work, while never forgetting trivial details. It is his insight and wide knowledge that guided me to the completion of this work. Due to his broad research interest, he gave me the opportunity to explore many interesting properties of the microstrip patch antennas.

I am also grateful to the support I received from the laboratory assistants in the Electrical and Computer Engineering department.

I also appreciate my secretary Mrs. Fana Molla, whose patience in typing the whole thesis manuscript adds me great strength

Last but not least I am greatly indebted to my family, especially to my mother who always encourages me to attain my goal.

TABLE OF CONTENTS

ABSTRACT

In this thesis work a single band microstrip patch antenna having a narrow operating bandwidth around the GSM900 band is designed. Theoretical analysis and design was performed by the Finite Difference Time Domain (FDTD) method based on the electromagnetic field solver Empire software.

To achieve the multiband antenna that can operate well in the: GSM (Global systems for mobile communication, 890-960 MHz), DCS (Digital cellular systems, 1710-1880 MHz), PCS (Personal Communication services, 1850-1990MHz), and UMTS (Universal Mobile Telecommunications Systems, 1920-2170MHz) bands. One needs to fine-tune the microstrip element to get dual band (GSM900 and GSM1800 bands) operation and to get a third or more operating band, one need to apply a shorted parasitic patch that is electromagnetically
coupled to the main radiator. The multiband antenna posses 14-dB around the GSM 900 band of operation and greater than 8-dB return loss with bandwidths enough to cover the intended higher operating bands. As the proposed antenna can achieve such wide operating bandwidth with relatively low profile, it is very suitable for multi-band mobile communication handsets.

Introduction

Introduction

Since the dawn of civilization, communication has been of foremost importance to mankind. In first place, communication was accomplished by sound trough voice. However, as the distance of communication increased, numerous devices were introduced, such as horns, drums, and so forth.

The radio antenna is a primary component in all radio systems. It may be defined as the structure associated with the region of transition between a guided wave and a free space wave, or vice versa [1]. In other words, radio antennas couple electromagnetic energy from one medium (space) to another (e.g. wire, coaxial cable, or wave guide).

Microstrip antennas appeared as a by-product of microstrip circuits, which by then had become a mature technology. Their design and realization took advantage of the techniques developed for microstrip circuits and used microstrip circuit substrates.

The increasing demand of multiband personal communications handsets fosters development of small-size integrated multiband antennas. The preferred solutions are usually metallic patches with multiple resonances. These patches allow a great flexibility in the antenna design, as they are cost–effective and straight forward to produce, as well as easy to adapt to the shape of the handset.

The demand for high performance multi-standard communication handsets has led to the research and studies of this interesting topic. Therefore, it is important to study the basic concepts of multiband antenna systems, a system that brings the world of wireless communication to a new era.

The first leap to understanding multiband microstrip patch antenna systems lead to the fundamental studies on antenna theory and their design parameters. Laying a good foundation is essential, as we will go through examining the multiband antenna system.

The radiation patterns and input return loss of the mutiband microstrip patch antennas at different resonant frequencies will have to be investigated and thus, further research will be carried out to bring a better insight by simulation methods. The area of study will conclude with analysis on simulations for the multiband microstrip antenna system. Hence, our aim is not only to analyze and study multiband microstrip antenna systems but also to study how the system can increase the capacity of wireless communication system by making the antennas and the system as a whole as a multi-standard device.

The thesis will begin with an introduction on antennas, describing the fundamental antenna parameters and makes a brief description of microstrip antennas in chapter one.

Chapter two will totally be devoted to the microstrip antennas, that is, its working principle and design techniques, analysis of microstrip antennas, feeding techniques and linearly polarized microstrip antennas will be dealt with. Chapter three discusses the design and simulation of single band microstrip antenna, which operates around GSM900 band.

The main body of the thesis that is the design and simulation of multiband microstrip patch antennas will be seen in chapters four and five. All simulations performed on multiband operation and the results will be presented.

Finally, chapter six draws a summary and concludes the thesis with the indication to possible future work.

Chapter 1

Antennas

1.1 Introduction

Communications has become the key to momentous changes in the organization of businesses and industries as they themselves adjust to the shift to an information economy. Information is indeed the lifeblood of modern economies and antennas provide mother earth a solution to a wireless communication system [5].

The radio antenna is an essential component in any radio system. An antenna is a device that provides a means for radiating or receiving radio waves. In other words, it provides a transition from guided waves on a transmission line to a “free space” wave (and vice versa in the receiving case). Thus information can be transferred between different locations without any intervening structure. Further more, antennas are required in situations where it is impossible, impractical or uneconomical to provide guiding structures between the transmitter and the receiver.

A guided wave traveling along a transmission line, which opens out as in figure 1.1, will radiate as free space wave. The guided wave is a plane wave while the free space wave is an spherically expanding wave [1]. Along the uniform part of the line, energy is guided, as a plane wave with little loss, provided the spacing between the wires is a small fraction of a wavelength. At the right, as the transmission line separation approaches a wavelength or more, the wave tends to be radiated so that the opened-out line acts like an antenna, which launched the free space wave. The currents on the transmission line flow out on the transmission line and end there, but the fields associated with them keep on going. To be more explicit, the region of transition between the guided wave and the free space wave may be defined as an antenna.

In this vast and dynamic field, the antenna technology has been an indispensable partner of the communication revolution. Many major advances that took place over the years are now in common use. Despite numerous challenges, the antenna technology has grown with a fast pace to haransse the electromagnetic spectrum, which is one of the greatest gifts of nature.

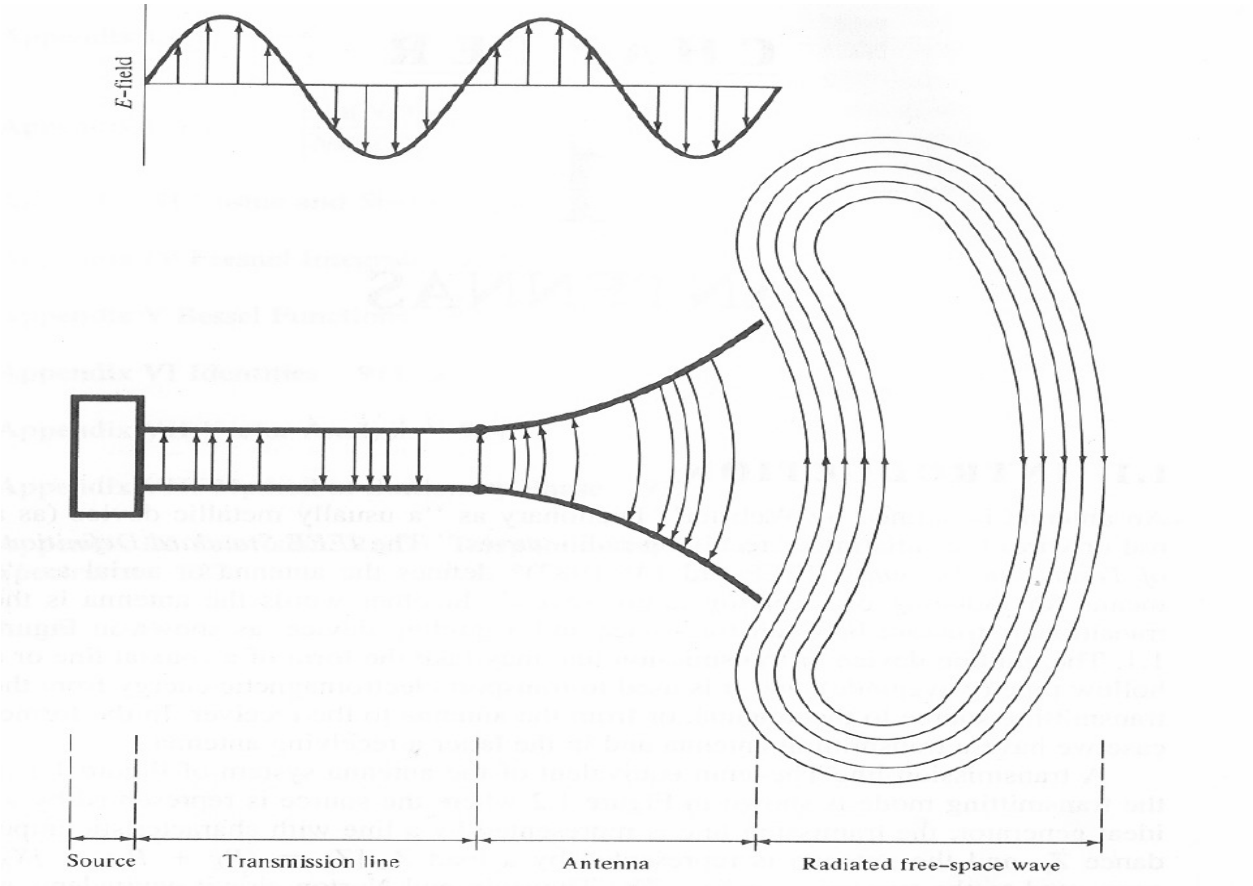

Figure 1.1.Antenna as a Transition Device [1]

1.2. Brief review of maxwell's equations

Maxwell's equations with the constitutive relations [5] are

Differential form	Integral form	
$\nabla \times E = \frac{\partial B}{\partial t}$	$\oint_c E.dl = -\int_s \frac{\partial B}{\partial t}.ds$	
$\nabla \times H = J + \frac{\partial D}{\partial t}$	$\oint_c H.dl = J + \int_S (\frac{\partial D}{\partial t}).ds$	(1.1)
$\nabla . B = 0$	$\oint_s B.d = 0$	
$\nabla . D = \rho$	$\oint_s D.ds = Q$	

The antenna problem consists of solving the fields that are created by an impressed current distribution, **J**. In the simplest approach, this current distribution is obtained during the solution process. But, if we assume that we have the current distribution and

wish to determine the fields **E** and **H**, we need only deal with the two curl equations of Maxwell's equations given above [5].

1.3. Types of Antennas

There are various types of antennas and they include wire antennas, aperture antennas, reflector antennas, lens antennas, microstrip antennas and array antennas. However, after giving a brief idea on wire antennas, aperture antennas, reflectors and lens antennas emphasis will be given to microstrip patch antennas [1].

Wire antennas: characterized by a presumed known current distribution, these are the oldest and still the most prevalent of all antenna configurations and they can be seen virtually anywhere. There are different shapes of wire antennas such as a straight wire (dipole), loop and helix.

Aperture antennas: characterized by a presumed known E-field distribution,they are most utilized for higher frequencies and antenna of this class are very useful for aircraft and space craft applications because they can easily be flush mounted onto the surface of the aircraft or space craft. Furthermore, they can be coated with a dielectric material to cushion them from hazardous conditions of the environment.

Reflector antennas are sophisticated forms of antennas used for communications over long distances. They are large in dimensions as to achieve high gain required to transmit or receive signals after millions of miles travel.

Lenses are mainly employed to collimate incident divergent energy to prevent it from spreading in undesired directions. Proper modeling of the geometrical configuration and using the correct materiel for the lenses can transform various forms of divergent energy into plane waves and these lens antennas are used in most of the applications of higher frequencies.

1.4. Basic Antenna Parameters

Definitions of various parameters are necessary to describe the performance of an antenna. Although the parameters may be interrelated, it is however, not a requirement to specify all the parameters for complete description of the antenna performance. An antenna is chosen for operation in a particular application according to its physical and electrical characteristics. Furthermore, the antenna must perform in a required mode for the particular measurement system.

An antenna can be characterized by the following parameters, not all of which apply to

all antenna types [1]:

1. Radiation pattern
2. Radiation resistance
3. Beam width and gain of main lobe.
4. Position and magnitude of side lobes.
5. Magnitude of back lobe.
6. Bandwidth
7. Aperture
8. Antenna correction factor
9. Polarization of the electric field that it transmits or receives
10. Power that the antenna can handle
11. Efficiency.

Typically, antenna characteristics are measured in two principal planes and they are known as azimuth and elevation planes, which can also be considered as the horizontal and vertical planes. Conventionally, the angle in the azimuth plane is denoted by the Greek letter phi (ϕ) while the Greek letter theta (θ) represents the angle in the elevation plane. Not all of the antenna characteristic factors will be discussed here. The following subsection will touch on some of the antenna parameters, which are essential for the understanding of the thesis.

1.4.1. Radiation Pattern

The antenna, which radiates or receives the electromagnetic energy in the same way, is a reciprocal device. Radiation pattern is very important characteristic of an antenna. It facilitates a stronger understanding of the key features of an antenna that otherwise cannot be achieved from the textual technical description of an antenna.

A radiation pattern (antenna pattern) is a graphical representation of the radiations (far-field) properties of an antenna. To completely specify the radiation pattern with respect to field intensity and polarization, three patterns are required [1].

1. The θ component of the electric field as a function of the angles θ and ϕ or $E_\theta(\theta,\phi)$. (Volt/meter)

2. The ϕ component of the electric field as a function of the angles θ and ϕ or E_ϕ (θ,ϕ). (Volt/meter)

3. The phases of these fields as a function of the angles θ and ϕ or $\delta_\theta(\theta,\phi)$ and $\delta_\phi(\theta,\phi)$. (degree or radian)

Although the radiation characteristics of an antenna involve three-dimensional patterns, many important radiation characteristics can be expressed in terms of simple single valued scalar quantities. These include:

-Beamwidths, beam area, main-lobe beam area and beam efficiency; directivity and gain

-Effective aperture, scattering aperture, aperture efficiency and effective height.

The radiation pattern can be plotted using rectangular/Cartesian or polar coordinates. The rectangular plots can be read more precisely (since the angular scale can be enlarged), but the polar plots offer a more pictorial representation and are thus easier to visualize.

1.4.1.1 Rectangular /Cartesian plots

Rectangular /Cartesian plots are standard x-y plots where the axes are plotted at right angle to each other. In a radiation plot, the angle with respect to bore sight is varied and the magnitude of the power radiated is measured; thus the angle is the independent variable and the power radiated is the dependent variable, A typical rectangular plot of an antenna radiation pattern is shown in Fig.1.2.

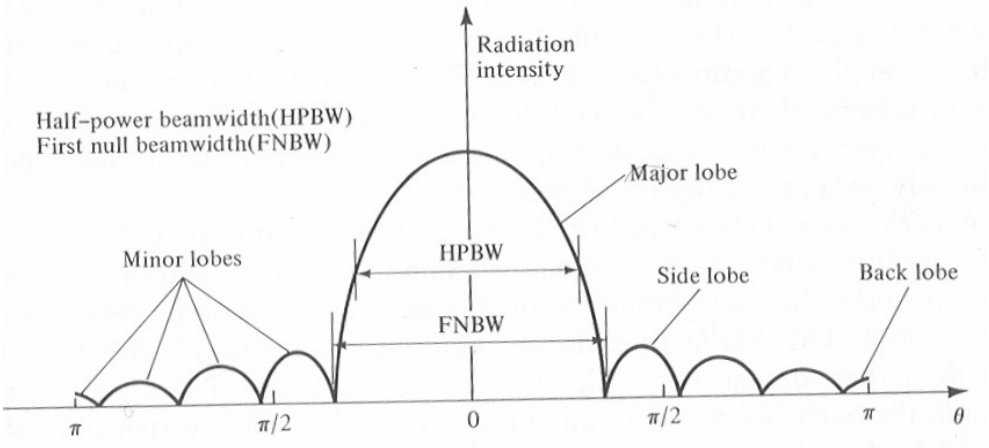

Fig 1.2- Rectangular Plot of an Antenna Pattern [1]

1.4.1.2. Polar Plots

In polar plot, the angles are plotted radially from bore sight and the power or intensity is plotted along the radius as shown in figure 1.3

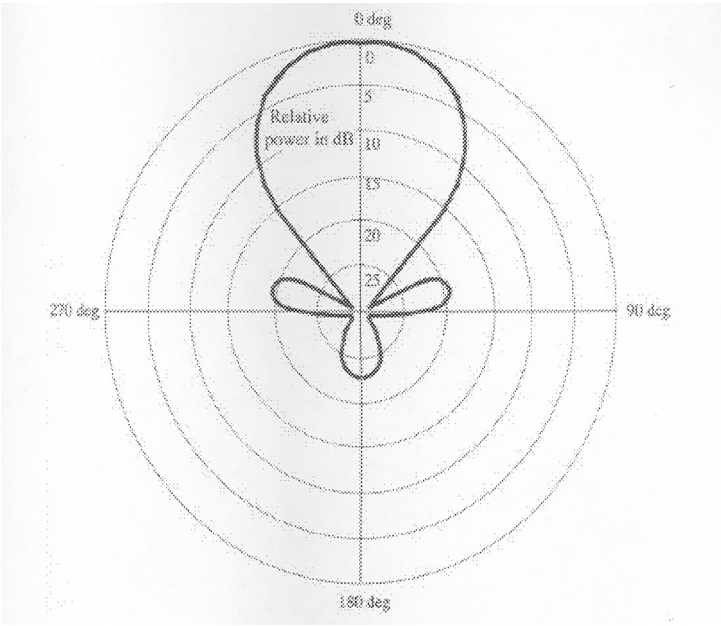

Figure 1.3-Typical Polar Plot of an Antenna [1]

This gives a pictorial representation of radiation pattern of the antenna and is easier to visualize than the rectangular/Cartesian plots. Although the accuracy cannot be increased as in the case of rectangular plot because the scale of the angular positions can only be plotted from 0^0 to 360^0, however, the scale of the intensity of power can be varied.

Each circle on the polar plot represents a contour plot where the power has the same magnitude and is shown relative to the power at bore sight. These levels will always be less than the power at bore sight and values should be shown as negative because the power in general is maximum at bore sight. However, they are normally written without a sign and should be assumed to be negative, contrary to standard arithmetic convention.

1.4.2. Half-power Beam Width

The half-power beamwidth is defined as: "In a plane containing the direction of the maximum of a beam, the angle between the two directions in which the radiation intensity is one-half the maximum value of the beam." Often the term beamwidth is used to describe the angle between any two points on the pattern such as the angle between the 10-dB points [5].

The beam width of the antenna is a very important figure of merit, and it often used as a tradeoff between the bandwidth and the side lobe level; that is, as the bandwidth decreases the side lobe increases and via versa [1].

1.4.3 Beam Efficiency

Beam efficiency is another parameter that is frequently used to judge the quality of transmitting and receiving antennas. For an antenna with its major lobe directed along the z-axis (θ=0 degree), as shown in Fig. 1.4.a below, the beam efficiency (BE) is defined as

$$\text{BE} = \frac{power transmitted (received) within cone angle \theta}{power transmitted (received) by the antenna} \qquad \text{(dimension less)} \quad (1.2)$$

Where θ is the half-angle of the cone with in which the percentage of the total power is to be found.

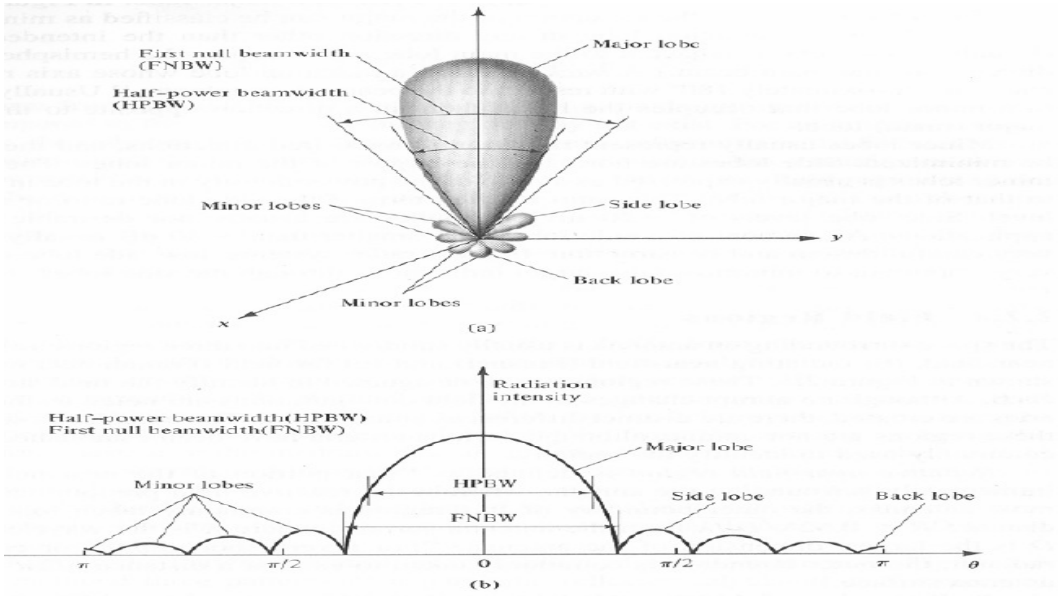

Figure 1.4. (a) Radiation Lobes and Beam Widths of an Antenna Pattern. (b) Linear Plot of Power Pattern and its associated Lobes and Beamwidths [1]

1.4.4. Bandwidth

The Bandwidth of an antenna is defined as "the range of frequencies within which the performance of the antenna, with respect to some characteristics, conforms to a specified standard". The bandwidth can be considered to be the range of frequencies, on either side

of a center frequency (usually the resonance frequency for a dipole), where the antenna characteristics (such as input impedance, pattern, beam width, polarization, side lobe level, gain, beam direction, beamwidth, radiation efficiency) are within an acceptable value of those at the center frequency.

For narrow band antennas, the bandwidth is expressed as a percentage of the frequency difference (upper minus lower) over the center frequency of the bandwidth [1].

1.4.5. Polarization

Polarization of an antenna in a given direction is defined as "the polarization of the wave radiated by the antenna. Note: when the direction is not stated, the polarization is taken to be the polarization in the direction of maximum gain."

Polarization of a radiated wave is defined as "that property of an electromagnetic wave describing the time varying direction and relative magnitude of the electric field vector: specifically, the figure traced as a function of time by the extremity of the vector at a fixed location in space, and the sense in which it is traced, as observed along the direction of propagation." Polarization then is the curve traced, by the end point of the arrow representing the instantaneous electric field [1]. A typical trace as a function of time is shown in figure 1.5.

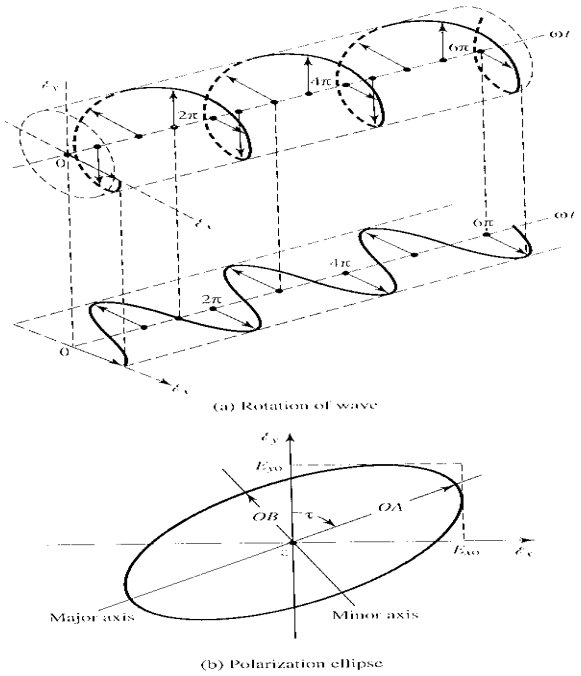

Figure 1.5. Rotation of a Plane Electromagnetic Wave and its Polarization Ellipse at z=0 as a function of time [1]

Polarization may be classified as linear, circular, or elliptical. If the vector that describes the electric field at a point in space as a function of time is always directed along a line, the field is said to be linearly polarized. In general, however, the figure that the electric field traces is an ellipse and the field is said to be elliptically polarized [1]. Linear and circular polarizations are special cases of elliptical, and they can be obtained when the ellipse becomes a straight line or a circle respectively.

The rotation of the electric field vector is traced in clockwise (cw) or counter clockwise (ccw) sense. Clockwise rotation of the electric field vector is designated as right hand polarization and counter clockwise as left hand polarization.

1.4.6. Directivity, gain, and Beam width

The directive gain of an antenna system towards a given direction (θ,ϕ) is the radiation intensity normalized by the corresponding isotropic intensity, that is [12]

$$D(\theta,\phi) = \frac{U(\theta,\phi)}{U_I} \tag{1.3}$$

Where U (θ,ϕ) is the radiation intensity, which is defined to be the power radiated per unit solid angle of the antenna system under consideration, and U_I is the radiation intensity of an isotropic antenna.

The directive gain measures the ability of the antenna to direct its power towards a given direction. The maximum value of the directive gain, D_{max}, is called the directivity of the antenna and will be realized to wards some particular direction, say (θ_O,ϕ_O). The radiation intensity will be maximum towards that direction, $U_{max} = U(\theta_O,\phi_O)$, so that

$$D_{max} = \frac{U_{MAX}}{U_I} \tag{1.4}$$

Another useful concept is that of the beam solid angle of an antenna. The definition is motivated by the case of a highly directive antenna, which concentrates all of its radiated power p_{rad} into a small solid angle $\Delta\Omega$ [12]

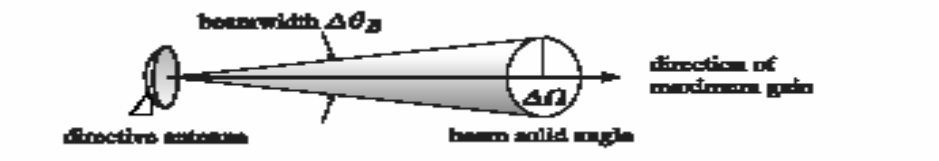

Figure 1.6. Beam Solid Angle and Beamwidth of a Highly Directive Antenna [12]

The radiation intensity in the direction of the solid angle will be:

$$U = \frac{p_{rad}}{\Delta\Omega} \tag{1.5}$$

It follows that: $$D_{max} = \frac{4\pi U}{P_{rad}} = \frac{4\pi}{\Delta\Omega} \tag{1.6}$$

1.5. Theory of Small Antennas

The small antennas studied in this thesis are resonators. Because a small antenna stores a relatively large amount of energy, its input impedance has a large reactive component in addition to a small radiation resistance. To deliver power to (and from) the antenna, it must be tuned to resonance, i.e. the input reactance must be cancelled out. Sufficient reactance cancellation can only occur inside a narrow bandwidth. In addition, the resonant resistance must be transformed to match the characteristic impedance of the feed line. A small antenna can be tuned to resonate with an appropriate additional reactance, or it can be made to self-resonate so that the reactance cancellation at resonance happens naturally in the antenna structure.

In the following, some theory of electrically small antennas is briefly discussed. The purpose is to define the most important terms and to explain what will happen when the antenna size is reduced, since miniaturization is the key word for the antenna designer of this wireless era.

1.5.1. QUALITY FACTOR

The quality factor of a resonator describes the rate at which energy decays in the resonator [13]. It is defined as

$$Q = \frac{\omega_r \times energystored\,\text{int}\,heresonator}{decreaseofenergypersec\,ond} = 2\pi f_r \frac{W}{P_l} \tag{1.7}$$

Where ϖ_r is angular resonant frequency, f_r is resonant frequency, w is stored energy, and P_l is power loss. At the resonant frequency, the electric and magnetic energies of the resonator are equal. The loss power can be divided into several load components, each of which can be described with a separate quality factors. The total quality factor is called the loaded quality factor (Q_l). It can be divided into the unloaded quality factor (Q_o) and the external quality factor (Q_e), as shown by equation (1.8). The unloaded quality factor describes the internal losses of the resonator, which can be further divided into radiation, conductor, and dielectric losses. These are described by radiation (Q_r), conductor (Q_c), and dielectric (Q_d) quality factors respectively. One or more external quality factors can be used to describe the losses caused by external connections to the resonator, such as the antenna feed [13].

$$\frac{1}{Q_l} = \frac{1}{Q_o} + \frac{1}{Q_e} = \frac{1}{Q_r} + \frac{1}{Q_d} + \frac{1}{Q_e} \tag{1.8}$$

The unloaded quality factor of a resonator can be determined from a simulated or measured frequency response of reflection coefficient.

1.5.2. BANDWIDTH

The useful bandwidth of an antenna may be limited by several factors, such as impedance, gain, polarization, or beamwidth. The input impedance is generally the main factor limiting the usable bandwidth of small antennas. The input impedance of a small antenna varies rapidly with frequency. This limits the frequency range over which the antenna can be matched to its feed line.

Impedance bandwidth is usually specified in terms of a return loss (L_{rten}) or voltage standing wave ratio (*VSWR*). Typical matching requirements are *VSWR* ≤2 or L_{retn} ≥10 dB [1]. Usually, the matching requirement is set in each case separately to meet the requirements of the application at hand. In recent years, L_{retn} ≥ 6dB(*VSWR* ≤3) has become a typical requirement for small internal antennas of mobile phones .Near resonance, the input impedance of a small antenna can be modeled by a parallel or series Resistance-Inductance-Capacitance(RLC) lumped-element equivalent circuit. By using a resonant circuit model, it can be shown that the relative impedance bandwidth Br of a small antenna is inversely proportional to its unloaded quality factor:

$$B_r = \frac{1}{Q_o}\sqrt{\frac{(TS-1)(S-T)}{S}} \tag{1.9}$$

Where S is maximum allowed voltage standing wave ratio (VSWR[S), and T is coupling coefficient. For a parallel resonant circuit, the coupling coefficient is calculated from $T = Y_0/G_0$, where Y_0 is the characteristic admittance of the feeding transmission line and G_0 is the resonant conductance of the antenna. For a series resonant circuit, the coupling coefficient is calculated from $T = Z_0/R_0$, where Z_0 is the characteristic impedance of the feeding transmission line, and R_0 is the resonant resistance of the antenna.

1.5.3. Minimum Radiation Quality Factor of a Small Antenna

The minimum radiation quality factor and the maximum bandwidth of an ideal single resonant small antenna are ultimately limited by the antenna size. The fields outside a virtual sphere (radius a), which completely encloses an antenna structure or an arbitrary current distribution, can be expressed with a complete set of orthogonal, spherical wave functions (spherical TM_{mn} and TE_{mn} wave modes). The space outside the virtual sphere can be thought of as a spherical wave-guide where the waves propagate in the radial direction. The cutoff radius of the spherical wave-guide is $r_c \cong n\lambda_o/2\pi$, where n is the mode number. The cutoff radius is independent of the mode number n. All the modes excited by the antenna contribute to the reactive power while only the propagating modes contribute to the radiated power. When the sphere around the antenna decreases, the number of propagating modes decreases and Q_r increases. When the sphere becomes small enough, even the lowest mode (n=1) becomes evanescent (non-propagating), and Q_r increases rapidly, as evanescent modes contribute very little to the radiated power.

With the use of the spherical wave modes, it is shown that of all linearly polarized small antennas, the lowest possible Q_r is obtained with an antenna that excites only either one of the lowest modes (TM_{01} or TE_{01}) outside the enclosing virtual sphere and stores no energy inside it. The theoretical minimum Q_r of such an antenna can be calculated from

$$Q_r = \frac{1}{(ka)^3} + \frac{1}{ka} \tag{1.10}$$

Where k is wave number ($k = 2\pi/\lambda o$), and a is the radius of the smallest sphere enclosing the antenna. In practice, however, all the antennas store energy also within the enclosing sphere, which increases their Q_r. Thus, equation (1.10) represents a fundamental lower limit, which is not reached with practical linearly polarized antennas.

According to equation (1.10), the radiation quality factor of an ideal small antenna is approximately inversely proportional to the volume of the antenna in wavelengths ($V/\lambda o^3$). Based on the spherical wave mode theory, practical small antennas such as shorted patches, must behave qualitatively the same way as the ideal antenna. The radiation quality factors of practical antennas are just higher, as explained above.

When both TM_{01} and TE_{01} modes are equally excited, as in circularly polarized small antennas, the theoretical minimum Q_r is about half of that obtained when only TM_{01} or TE_{01} mode is excited. The theoretical minimum Qr of an ideal small antenna, with TM_{01} and TE_{01} modes equally excited, can be calculated from:

$$Q_r = \frac{1}{2\,(ka)^3} + \frac{1}{ka} \tag{1.11}$$

Generally, to minimize Qr, the antenna structure should use the space inside the enclosing sphere as efficiently as possible. For example, the Q_r of the PIFA is known to decrease as its height increases. The height of a basic PIFA can be increased without increasing the radius of the enclosing sphere, because the condition for its fundamental resonance is related to its length (l) and height (h) as $l + h = \lambda/4$. Therefore, it can be argued that increasing the height of a PIFA makes its Qr approach the theoretical limit because the antenna utilizes the volume of the enclosing sphere more efficiently.

1.5.4. EFFICIENCY

Total antenna efficiency (η_t) measures how well an antenna converts the input power available at the antenna feed to radiated power (P_r), which can be measured in the far field. The total efficiency can be divided into radiation efficiency (η_r) and reflection (mismatch) efficiency (η_{reff}):

$$\eta_t = \eta_r \eta_{erff} \tag{1.12}$$

Radiation efficiency tells how much of the input power accepted by an antenna (P_{in}) it converts to radiated power. Radiation efficiency can also be expressed as the ratio of the unloaded quality factor to the radiation quality factor of the antenna. As shown by equations (1.8) and (1.9), if Q_r increases, Q_c and Q_d must be increased accordingly, otherwise the radiation efficiency decreases. For a given radiation efficiency, a narrowband antenna requires the use of less lossy materials than a wideband antenna.

$$\eta_r = P_r/P_{in} = Qo/Q_r \tag{1.13}$$

Proper matching ensures that a desired amount of the available power is transferred into the antenna. Reflection efficiency is defined as

$$\eta_{erfl=}1-/\Gamma/^2 \quad (1.14)$$

Where Γ is voltage reflection coefficient at the antenna feed. It can be calculated from

$$\Gamma=(Z_{in}-Z_o)/(Z_{in}+Z_o) \quad (1.15)$$

Where Z_{in} is antenna input impedance, and Z_0 is characteristic impedance of the feed line

The typical radiation quality factors of the antennas studied in this thesis are small enough and the materials are so good (Qc and Q_d sufficiently high) that the radiation efficiency is not the main factor limiting the total efficiency of the antennas. The total efficiency is mainly limited by the reflection efficiency at the edges of the operation band.

1.6. Bandwidth Enhancement of Small Antennas

In the following, the bandwidth enhancement of small resonant antennas will be discussed using short–circuited microstrip patch antennas as models.

1.6.1. Increasing Element Size

The impedance bandwidth of a small antenna is greatly limited by its electrical size. Therefore, an obvious way to improve the performance is increasing the antenna size [7]. For example, the impedance bandwidth of an open circuited patch antenna is known to increase as its width or height (substrate thickness) increases or the relative permittivity of its substrate decreases (length increases). Although effective increasing of antenna size is often impossible in small radio devices.

1.6.2. Reducing Efficiency

Besides increasing the size of a small antenna, its impedance bandwidth can be increased by reducing its efficiency artificially. This can be done, for example, by manufacturing the antenna from lossy material or by adding resistive components into the structure. By combining equations (1.9) and (1.13), it can be seen that the relative bandwidth is inversely proportional to the radiation efficiency. Thus, halving the radiation efficiency can double the impedance bandwidth. The obvious disadvantage of this method is reduction in antenna gain.

From the antenna design point of view, a simple way to improve the impedance bandwidth is to add an attenuator in series with the antenna. For example, adding a 3-dB attenuator will theoretically lead to a 6-dB return loss over an infinitely wideband, but it will also reduce the total efficiency by 3-dB [7].

Another way of obtaining a larger impedance bandwidth at the expense of efficiency is simply by accepting a smaller return loss. For example, by using equation (1.9), it can be estimated that accepting a return loss of 6-dB instead of 10-dB will increase the impedance bandwidth of a single resonant antenna by a factor of 1.7. This decreases the total efficiency of the antenna at the band edges by 0.8-dB [8].

1.6.3. Using Multiple Resonances

Use of multiple resonances is an effective method of increasing the impedance bandwidth of small resonant antennas. It enables a significant increase of bandwidth even when the antenna size and efficiency are fixed. A multiresonant small antenna can be obtained by adding one or more high–Q matching resonators or parasitic elements to the original antenna. In some antenna structures, it is also possible to excite two orthogonal resonant modes with close enough frequencies [8]. Generally, the bandwidth increases as the number of closely–tuned coupled resonances increases. The price for increased bandwidth with multiple resonances is increased design complexity. Adding resonators may also increase the manufacturing complexity and costs. Furthermore ohmic losses in the additional resonators can reduce the radiation efficiency.

1.6.3.1. High–Q Matching Resonators

A well-known method of increasing the impedance bandwidth of resonant antennas is adding a matching network, which consists of high Q (low –loss) resonators, between the antenna and the feed line [13]. The matching network may contain one or more resonators, and it can be separated from or integrated to the antenna structure.

There are fundamental limitations on the broadband impedance matching of a purely resistive source to a passive complex load, such as a small resonant antenna, with a reactive matching network. Many works on this concept show that regardless of the number of elements in the matching network, a perfect match cannot be obtained over the whole frequency spectrum or even at all frequencies within a finite frequency range. A perfect match can be obtained only at a finite number of frequencies but even in that case, the theoretical maximum bandwidth is limited by the inherent Q_0 of the load. Making the reflection coefficient very small at any point of the pass band decreases the theoretical maximum bandwidth. The best result is obtained if a less than a perfect match is accepted and a maximum tolerance, such as a maximum allowed reflection coefficient, is defined for the match. For example, a network is illustrated in figure1.7, with properly selected

element values, will increase the best VSWR, bandwidth of the patch element alone by a factor of about 2.84 [13].

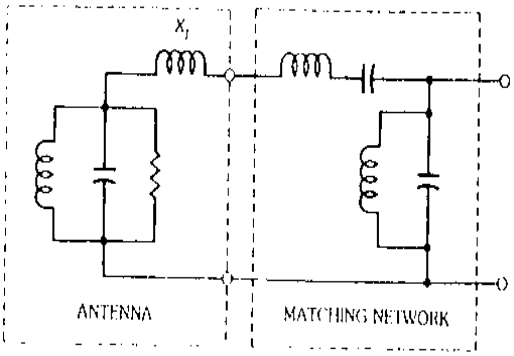

Figure 1.7.External-matching circuit for a microstrip element using two matching sections [13]

The section of the network in figure 1.7 that is enclosed by the dashed line represents the model of the input impedance of the microstrip element. One notes that part of the inductance required by the first matching section is supplied by the microstrip element itself. This inductive part can be significant, particularly for thicker elements and elements fed at high–inductance points.

The price for this improvement as explained earlier is a reduction in overall efficiency due to unavoidable losses in the matching filter. A greater price is the space that the matching network must occupy. The network can be realized using microstripline or Stripline elements. If the latter is used, the network can be placed in a second layer of the circuit board under the patch.

1.6.3.2. Parasitic Elements

Another general way of realizing a dual-resonant or multiresonant antenna is by adding one or more appropriately coupled parasitic elements into a single–resonant antenna structure. Matching resonators are typically non-radiating elements with high unloaded quality factors, whereas parasitic elements are designed to radiate. Their unloaded quality factors are typically of the same order as that of the driven element. Usually, the driven antenna element and the parasitic elements are of the same antenna type. However, in principle it is possible to combine any resonant antenna types. The bandwidth of a patch type antenna can be increased by adding one or more parasitic patch elements on the same plane as the driven patch, or on top of the driven patch. The former are here

referred to as coplanar parasitic elements and the latter as stacked parasitic elements. Like traditional single-resonant patch antennas, the driven and parasitic patches may have virtually any shape, which enables numerous configurations with slightly different characteristics. This makes, for example, fitting the antenna elements inside the covers of a mobile phone easier.

Coplanar parasitic elements can be coupled either to the radiating or non-radiating edges of the driven patch or both. Typically coplanar parasitic elements have been separated from the driven element by a narrow gap, but to increase the coupling, they can also have a direct (galvanic) contact to it. In addition to increasing bandwidth, a major advantage of the coplanar configuration is easy fabrication because only one dielectric layer is required. Increased surface area and antenna size are often stated as disadvantages of coplanar parasitics. However, it has been shown in many previous works that the bandwidth of a short-circuited patch antenna can be increased by a factor of around two without increasing its size by dividing the original patch into two properly tuned and coupled narrower strips, of which one is fed and the other one is parasitic. Thus, a significant improvement can be obtained without increasing the surface area or the volume occupied by the antenna. Even larger improvements can be obtained by increasing the antenna size. One potential problem of patches with coplanar parasitics is that their radiation characteristics can change with frequency, especially if the antenna is not symmetric [8].

Stacked parasitic elements were first used with open-circuited patches. The stacked configuration may be more difficult to manufacture than the coplanar one because of the additional metal layers. On the other hand, it is possible to use different substrates in different layers, which may help in the performance optimization. Increased antenna thickness can be seen as disadvantage of the stacked configuration. Generally, the radiation characteristics of the stacked configuration can be preferred to those of the coplanar ones because similar frequency dependent changes as those reported in the case of coplanar parasitics have not been observed with typical stacked configurations.

At the moment, there are no simple general equations enabling systematic design of dual-resonant and multiresonant patch antennas that have parasitic elements. Both simulated and experimental designs are obtained through trial and error. Despite the large number of papers reporting various dual-resonant and multiresonant antenna structures, there has

been a lack of a unified set of simple design and bandwidth optimization of all resonant antennas having parasitic elements. There are, however, papers where the effects of various geometry-related design parameters on the performance of dual resonant patches are discussed. In this thesis also, we start with the concepts and principles of designing microstrip patch antennas and try to reach multiband operations using the simulation software (i.e. the field slower EMPIRE) [9].

1.6.3.3. Excitation of Two Nearly Orthogonal Resonances

In some antenna structures, such as in suitably shaped open circuited patch antennas, the impedance bandwidth can be increased by exciting two resonant modes with equal resonant frequencies and unloaded quality factors. One of the modes is excited by the feed, whereas the other one is excited by a suitable perturbation in the patch shape. Such an antenna can be obtained for example from a linearly polarized, square shaped, open-circuited patch by removing a piece of the patch from one of the corners [13]. The coupling between the resonances is controlled by the size of the removed piece. The described wideband antenna structures are similar to those used as single-feed circularly polarized patch antennas. The coupling between the modes is adjusted for optimal circularly polarized radiation, whereas in the wideband antennas the coupling is optimized to maximize the bandwidth. With this antenna type, the impedance bandwidth can be increased much higher than that obtained with a high–Q matching resonator. The radiation characteristics of this type of wideband antenna change with frequency, which limits its applications. Furthermore, a square-shaped half-wave patch is more difficult to fit it inside a small radio device than a short- circuited quarter-wavelength patch.

1.7. Microstrip Antennas

Microstrip antennas became very popular in the 1970s primarily for space borne applications. They are low profile antennas that are being used in high-performance aircraft, spacecraft, satellite and missile applications, where size, weight, cost, performance, ease of installation and aerodynamic profile are constraints [13].

There are many different varieties of microstrip antennas, but their common feature is that they basically consist of four parts.

a) A very thin flat metallic region often called the patch;
b) A dielectric substrate;
c) A ground plane, which is usually much larger than the patch; and

d) A feed, which supplies the element radio frequency power.

Microstrip elements are often made by etching the patch (and sometimes the feeding circuitry) from a single circuit board clad with conductor on both of its sides. The longest dimension of the patch is typically about a third to a half of a free space wavelength (λo), while the dielectric thickness is usually in the range of $0.003\lambda o$ to $0.05\lambda o$ [13]. A commonly used dielectric for such antennas is poly tetra floural ethyhne (PTFE), often set in a reinforcing glass fiber matrix. A relative dielectric constant of 2.5 is typical. Sometimes a low-density cellular "honey comb" material is used to support the patch. This material has a relative dielectric constant much closer to unity and usually results in an element with better efficiency and larger bandwidth, though at the expense of an increased element size. Substrate materials with high dielectric constant can be used. For the radiation modes most used, however, such substrates result in elements, which are electrically small in terms of free-space wavelengths and consequently have relatively smaller bandwidths or low efficiencies [13].

The reasons why this class of antennas has become so popular include the following

1. They are low-profile antennas.
2. They are easily conformable to non-planar surfaces. Along with their low profile this makes them well suited for use on high-performance airframes.
3. They are easy and inexpensive to manufacture in large quantities using modern printed circuit techniques.
4. When mounted to a rigid surface they are mechanically robust
5. They are versatile elements in the sense that they can be designed to produce a wide variety of patterns and polarizations, depending on the mode excited and the particular shape of the patch used.
6. Adaptive elements can be made by simply adding appropriately placed pin or varactor diodes between the patch and the ground plane. Using such loaded elements one can vary the antennas resonant frequency, polarization, impedance, and even its pattern by simply changing bias voltages on the diodes.

These advantages must be weighed against the disadvantages, which can most succinctly stated in terms of the antennas quality factor, Q. Microstrip antennas are high-Q devices with Qs sometimes exceeding 100 for the thinner elements. High Q elements have small bandwidths. Also, the higher the Q of an element, the lower is its efficiency. Increasing

the thickness of the dielectric substrate will reduce the Q of the microstrip element and there by increase its bandwidth and its efficiency. There are limits, however, as the thickness is increased, an increasing fraction of the total power delivered by the source goes into a surface wave. This surface wave contribution can also be counted as an unwanted power loss since it is ultimately scattered at dielectric bends and discontinuities. Such scattered fields are difficult to control and may have a deleterious effect on the pattern of the element. One also needs to be aware that microstrip elements are modal devices. If the band of the element is so large that it encompasses the resonant frequencies of two or more resonant modes, the pattern is likely not to be stable throughout the band even though the VSWR at the input could be acceptably low.

Despite the disadvantages the advantages of microstrip antennas have led to their use in many applications in civilian and government systems. In fact, one so–called disadvantage, small bandwidth, is sometimes counted as an advantage instead. For narrow band applications the antenna itself can act as a filter for unwanted frequency components. Even with the relatively high Q these elements have, a sufficiently thick element with a well-designed external matching circuit can have a bandwidth as large as 35 percent. Finally, if surface-wave loss is not counted as an unwanted power loss (or does not exist because the dielectric is truncated or has a relative dielectric constant nearly unity), the efficiency of a sufficiently thick element can easily be made larger than 90 percent [13].

Microstrip antennas are classified into three basic types. Microstrip patch antennas, microstrip traveling-wave antennas, and microstrip slot antennas. The physical structure of the microstrip antennas is very simple and they may take the form of any geometrical shape and size Fig.1.7 shows some of the shapes of microstrip patch elements.

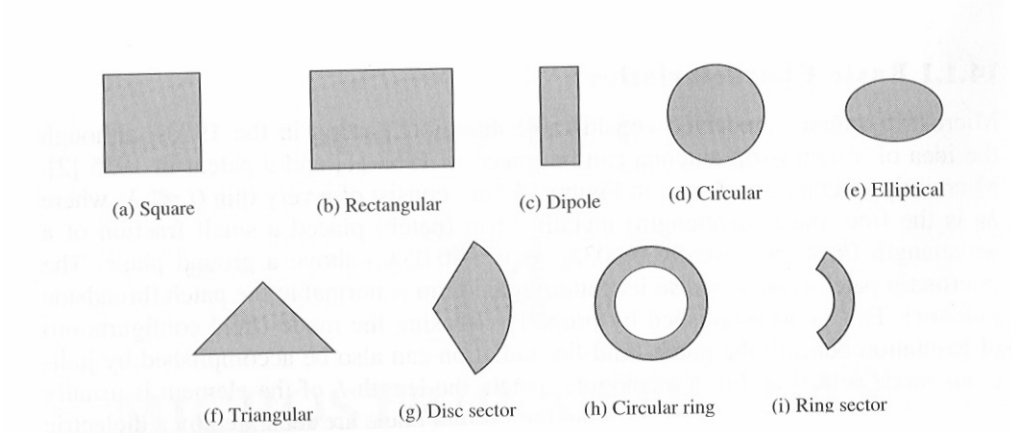

Figure 1.8. Representative Shapes of Microstrip Patch Elements [1]

However, rectangular and circular patches are most favorable, because of the ease in analysis and fabrication, and their attractive radiation characteristics, especially low cross-polarization radiation. Thus, rectangular microstrip antenna patches are chosen for our analysis.

In the next chapter, the design of conventional rectangular microstrip antenna is considered. Later on, some modifications will be made to make the antenna practical.

Chapter 2

MICROSTRIP ANTENNAS

2.1. Introduction

Microstrips are printed circuits operating in the microwave range, over the gigahertz region of the electromagnetic spectrum [7]. Realized by the photolithographic process, they let designers reduce the size, weight, and cost of components and systems for low signal-level applications by replacing the more cumbersome wave-guide components and assemblies. The fabrication process is well suited for series production of circuits and antennas, since lumped circuit and active devices can easily be combined with sections of transmission line. At microwave frequencies, all dimensions become important, so the realization of microstrips requires more care than that of low-frequency printed circuits.

Microstrip lines were first proposed in 1952 and were increasingly used in the late 1960s and 1970s to realize circuits, generally called microwave integrated circuits (MICs) since radiation leakage is most unwanted in circuits, particular care was taken to avoid it, even though its possible application to design antennas had already been suggested in 1953 [13]. Microstrip antennas appeared as a by-product of microstrip circuits, which by then had become a mature technology. Their design and realization took advantage of the techniques developed for microstrip circuits and used microstrip circuit substrates.

2.2. General Background

Microstrip devices are planar components for microwaves and high frequency electronics, which can replace bulky wave-guides whenever the frequency or the power level of signals permits. At low frequencies one uses open structures where as at high frequencies metal enclosures surround the circuits to avoid radiation [7].

These days, a plenty of various types of patch antennas are at our disposal. These antennas differ in the shape of the antenna elements (rectangular, circular, annular, etc), in polarization they operate with, in feeding techniques considered, etc.

Small impedance bandwidth is a common property of patch antennas. For classical patch antennas, the bandwidth is about 2 to 3 percent and for aperture fed antennas it is about 4 to 6 percent [7]. High quality factor of patches is the reason.

Antenna efficiency is another important parameter. Radiation efficiency (computed for lossless antenna) is given by the ratio of radiated power (integrating poynting vector in the far region over the whole half-space) and real power on the input port of the antenna. Energy, which is not radiated by the antenna, is taken away in the form of surface waves along the infinite dielectric substrate (in real situation, the substrate is limited, of course).

2.3. Microstrip Structures

A microstrip structure is made with a thin sheet of low-loss insulating material called the dielectric substrate. It is completely covered with metal on one side, called the ground plane, and partly metallized on the other side, where the circuit or antenna shapes are printed [7]. Components can be included in the circuit either by implanting lumped components (resistors, inductors, capacitors, semiconductors, and ferrite devices) or by realizing them directly with in the circuit.

Each part of the microstrip structure will be explained in detail as follows.

1. Dielectric Substrate

The Dielectric substrate is the mechanical backbone of the microstrip circuit. It provides a stable support for the conductor strips and patches that make up connecting lines, resonators and antennas. It ensures that the components that are implanted are properly located and firmly held in place, just as in printed circuits for electronics at lower frequencies.

The substrate also fulfills an electrical function by concentrating the electromagnetic fields and preventing unwanted radiation in circuits. The dielectric is an integral part of the connecting transmission lines and deposited components: its permittivity and thickness determine the electrical characteristics of the circuit or of the antenna.

2. Conductor Layers

Nowadays, many commercial suppliers provide a wide range of microstrip substrates, already metallized on both faces. The conductor on the upper face is chemically etched to realize the circuit pattern by a photographic technique. A mask of the circuit of the antenna is drawn, generally at convenient scale, and then reduced and placed in close contact with a photo resistive layer, which was previously deposited on top of the

metallized substrate. The lower metal part is the ground plane. The ground plane, besides acting as a mechanical support, provides for integration of several components and serves also as a heat sink and dc bias return for active devices. The resulting sandwich is then exposed to ultraviolet rays, which reach the photosensitive layer where it is not covered by the mask. The exposed parts are removed by the photographic development, and the metal cover is etched away from the exposed area. This process is called the subtractive process.

Alternately, one may wish to use a bare dielectric substrate as a starting material and deposit metal either by evaporation or by sputtering through the holes in the mask. This is called the additive thin-film process. In the thick-film process, a metallic paste is squeezed through the holes in a mask deposited over a silk screen. The latter approach, however, is less accurate and is seldom used at very high frequencies.

2.4. Waves on Microstrips

The mechanisms of transmission and radiation in a microstrip can be understood by considering a point current source (Hertz dipole) located on top of the grounded dielectric substrate as shown on figure 2.1 below. This source radiates electromagnetic waves. Depending on the direction toward which waves are transmitted, they fall within three distinct categories, each of which exhibits quite different characteristics

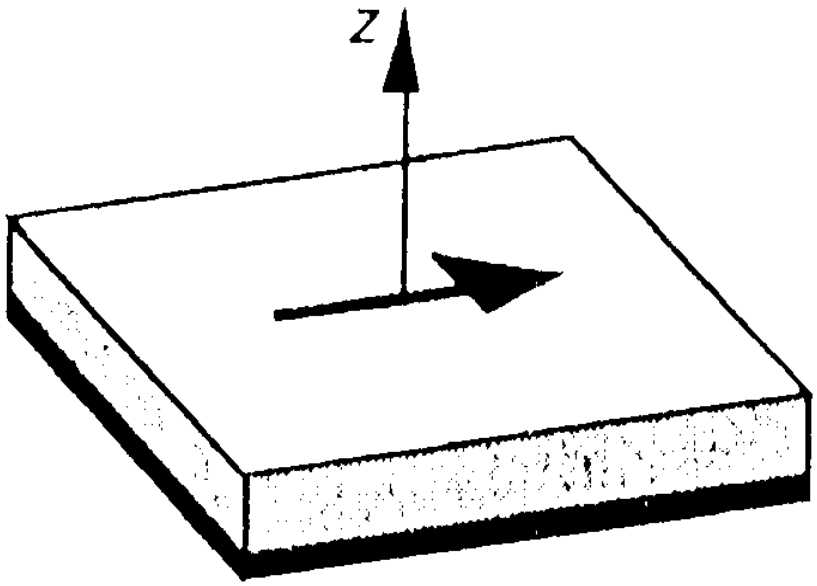

Figure: 2.1. Hertz on a Microstrip Substrate [7]

2.4.1. Space Waves

Waves transmitted upward, with elevation angles θ between 0 and $\pi/2$, move toward free open space above, where they do not find any further interfaces as shown in Fig.2.2 below.

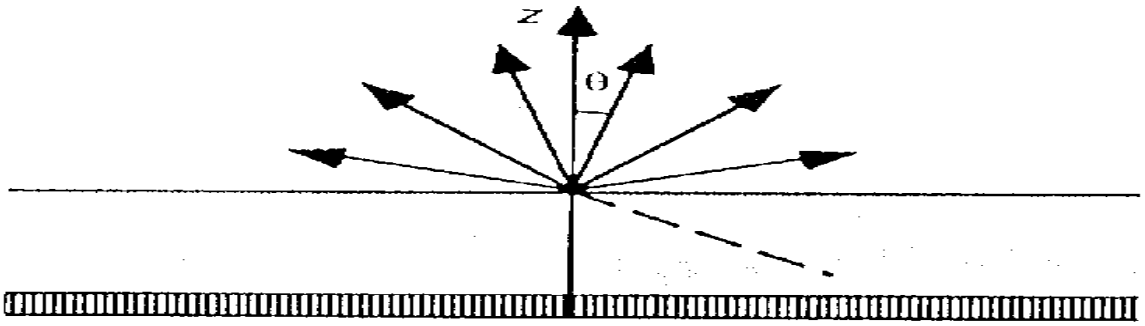

Figure 2.2 Radiated Waves [7]

These waves are thus radiated, with field amplitudes decreasing with distance (r), as 1/r. Space waves are essential for all applications, which specifically rely on radiation for their operation. In transmission lines and circuits, on the other hand, they produce spurious leakage and, therefore, undesirable.

2.4.2. Surface Waves

The waves transmitted slightly downward, having elevation angles θ between $\pi/2$ and π - arcsine $(1/\sqrt{\varepsilon_r})$, meet the ground plane, which reflects them, and then meet the dielectric-to-air boundary, which also reflects them (local reflection condition) [7]. Field amplitudes build up for some particular incidence angles, leading to the excitation of a discrete set of surface wave modes, similar to the modes in a metallic wave-guide.

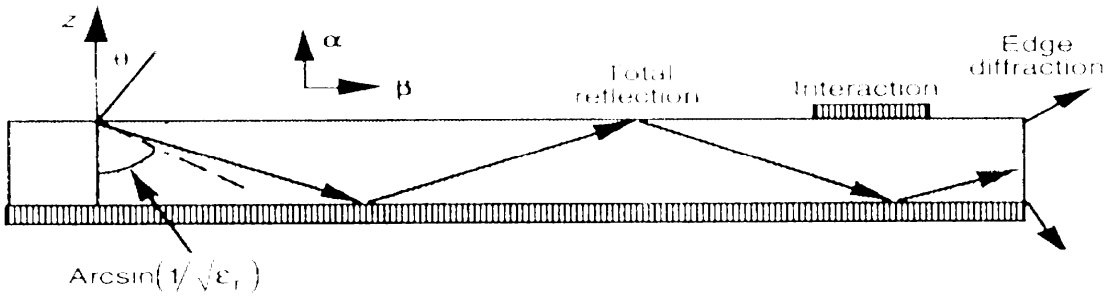

Figure 2.3. Surface Waves [7]

The fields remain mostly trapped with in the dielectric, decaying exponentially above the interface Fig.2.3. The vector α pointing upwards indicates the direction of largest attenuation. The wave propagates horizontally along β, with little absorption in good quality dielectric. With two directions of α and β orthogonal to each other, the wave is non-uniform plane wave. Surface waves spread out in cylindrical fashion around the excitation point, with field amplitudes decreasing with distance (r), say $1/\sqrt{r}$, more slowly than space waves. Surface waves take up some part of the signal's energy, which does not reach the intended user. The signal's amplitude is thus reduced, contributing to an apparent attenuation or a decrease in antenna efficiency.

Additionally, surface waves also introduce spurious coupling between different circuit or antenna elements. This effect of surface wave coupling becomes particularly obnoxious, and the array can neither transmit nor receive when it is pointed at some particular directions (blind spots). This is due to a resonance phenomenon, when the surface waves excite in synchronism the floquet modes of the periodic structure.

Surface waves reaching the outer boundaries of an open microstrip structure are reflected and diffracted by the edges. The diffracted waves provide an additional contribution to radiation degrading the antenna pattern by raising the side lobe and the cross polarization levels. Surface wave effects are mostly negative for circuits and for antennas, so their excitation should be suppressed if possible.

2.4.3. Leaky Waves

Waves directed more sharply downward, with θ angles between arcsin ($1/\sqrt{\varepsilon_r}$) and π, are also reflected by the ground plane but only partially by the dielectric- to-air boundary. They progressively leak from the substrate into the air Fig.2.4, hence their name leaky waves, and eventually contribute to radiation.

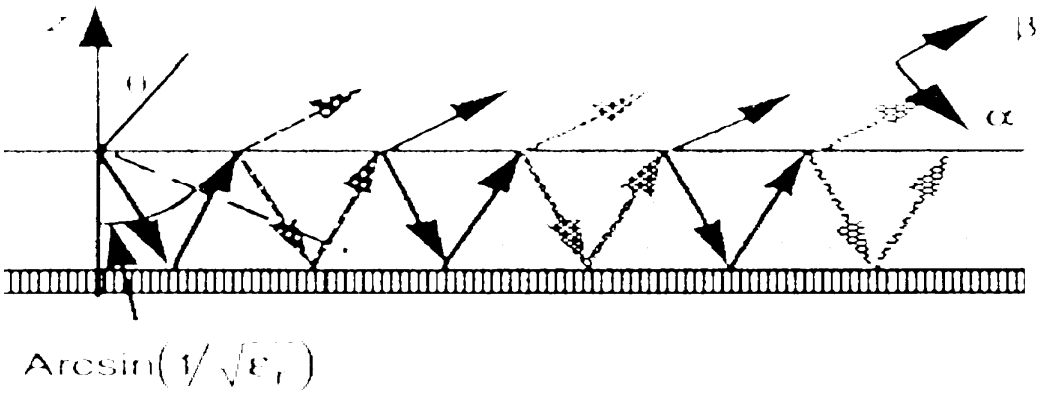

Figure: 2.4. Leaky Waves [7]

The leaky waves are also non-uniform plane waves for which the attenuation direction α points downward, which may appear to rather odd; the amplitude of the waves increases as one moves away from the dielectric surface. This apparent paradox is easily understood by looking at the figure; actually, the field amplitude increases as one moves away from the substrate because the wave radiates from a point where the signal amplitude is larger. Since the structure is finite, this apparent divergent behavior can only exist locally, and the wave vanishes abruptly as one crosses the trajectory of the first ray in the figure.

In more complex structures made with several layers of different dielectrics, leaky waves can be used to increase the apparent antenna size and thus provide a larger gain. This occurs for favorable stacking arrangements and at particular frequency. Conversely, leaky waves are not excited in some other multi layer structures.

2.4.4. Guide Waves

When realizing printed circuits, one locally adds a metal layer on top of the substrate, which modifies the geometry, introducing an additional reflecting boundary. Waves directed into the dielectric located under the upper conductor bounce back and forth on the metal boundaries, which form a parallel plate wave-guide Fig.2.5. The waves in the metallic guide can only exist for some particular values of the angle of incidence forming a discrete set of wave-guide modes.

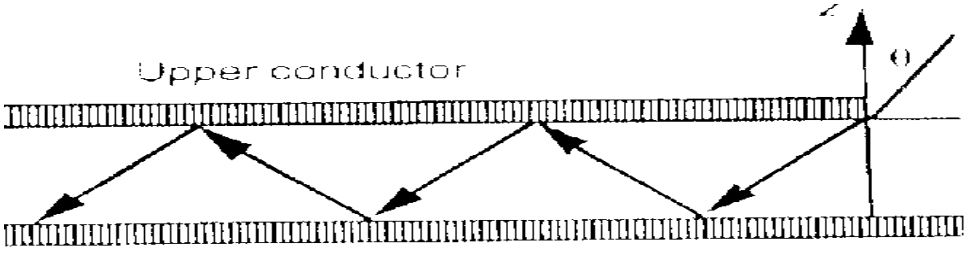

Figure2.5 Guide Waves

The guide waves provide the normal operation of all transmission lines and circuits, in which the electromagnetic fields are mostly concentrated in the volume below the upper conductor. On the other hand, this buildup of electromagnetic energy is not favorable for patch antennas, which behave like resonators with a limited frequency bandwidth.

2.5. Microstrip Antenna Types

2.5.1. Microstrip Dipole

The small size of the dipole antennas makes them attractive for many applications but also results in a very narrow frequency bandwidth. No transverse currents flow on a narrow dipole, so the cross-polarization level is inherently low.

A microstrip dipole is usually fed by a balanced feed, for instance, a parallel two-wire line printed on the substrate or two wires connected through the substrate. Transitions or baluns must then be incorporated to connect the feed to a microstrip line or to a coaxial line, which are both inherently unbalanced transmission lines. Alternately, dipoles may also be fed by electromagnetic coupling with embedded feed lines.

2.5.2. Microstrip Patch

Printed patch antennas use radiating elements of a wide variety of shapes. Square, rectangle, circle, ring, triangle, more complex geometrical figures and combinations of

simpler shapes are also used for some particular applications. The selection of a particular shape depends on the parameters one wishes to optimize bandwidth, side lobes cross polarization, and antenna size.

Microstrip patches present a somewhat broader relative bandwidth than dipoles, of the order of a few percent. In contrast to thin dipoles, patches may excite some surface current flowing across the transverse direction, which then radiates an unwanted cross polarized component. Its amplitude is critically dependent on the kind of feed and on its location with respect to the axes of the patch.

2.5.2.1. Rectangular Patches

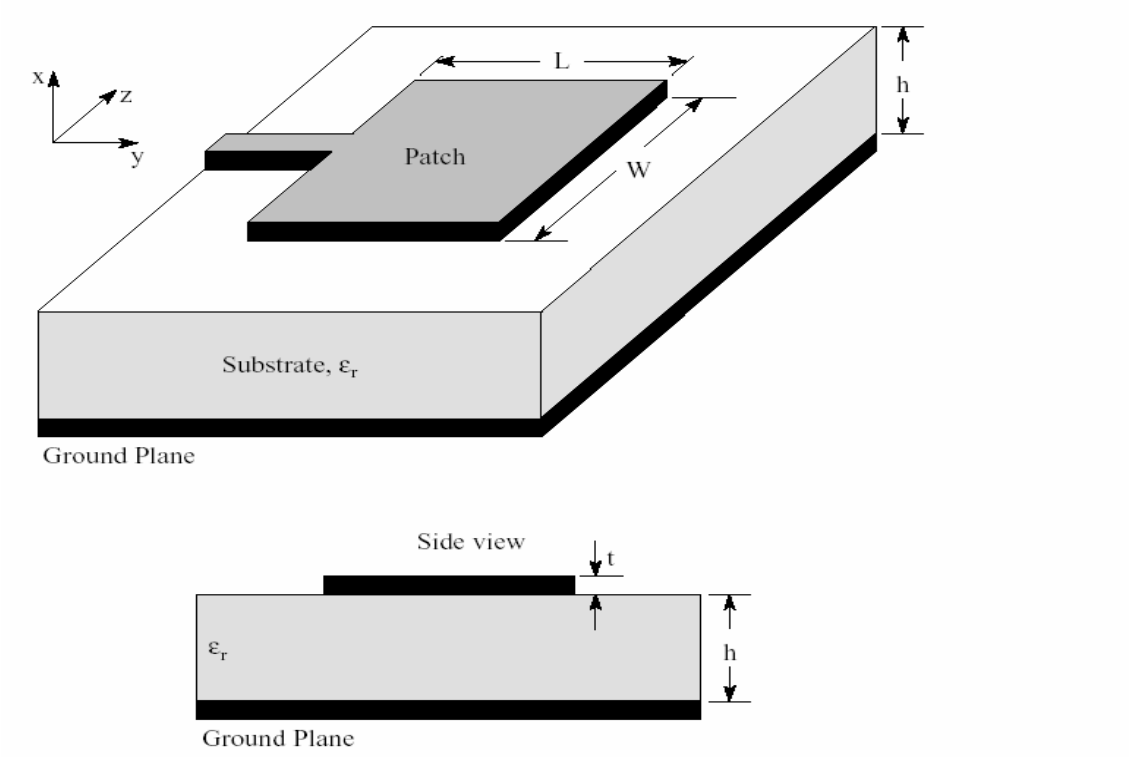

Figure 2.6 Geometry of Rectangular Microstrip Patch Antenna (not to scale) [1].

The geometrical shape most commonly used to realize microstrip patch antennas are the rectangle. A rectangular patch can be considered to be an open-ended section of transmission line of length L and width w as in Fig. 2.6.above.

The fringing fields at the two open ends are accounted for by adding equivalent length ΔL at both ends. Then, the resonant frequencies are provided by[7] :

$$f_m = \frac{m C_o}{2(L + \Delta L)\sqrt{\varepsilon_r}} \qquad (2.1)$$

With the integer m= 1,2,3,(≠0) and a relative permittivity ε_e given by equation(2.7),where Co is free space speed of light and εe is the effective permittivity of the substrate. Expression (2.1) is for resonant modes in which the surface current is mostly longitudinal, more complex resonance patterns are obtained for higher order modes on wide lines. The lines of surface current correspond, respectively, to the TM_{100}, the TM_{010}, and the TM_{110} modes for an equivalent square-shaped cavity having perfect magnetic conductor (PMC) side walls (see on cavity model).

2.5.2.2. Circular Patch

Circular patches were reported to lose less energy by radiation and thus provide larger quality factors than rectangular patches (this desirable feature for operation as a resonator in a circuit becomes a drawback when realizing antennas).The resonant frequency is determined by assuming that a perfect magnetic wall (PMC) extends under the edges of the patch as in Fig.2.7.below. Fringing fields are taken into account by defining an effective resonator radius a_e, which is slightly larger than the physical radius a.

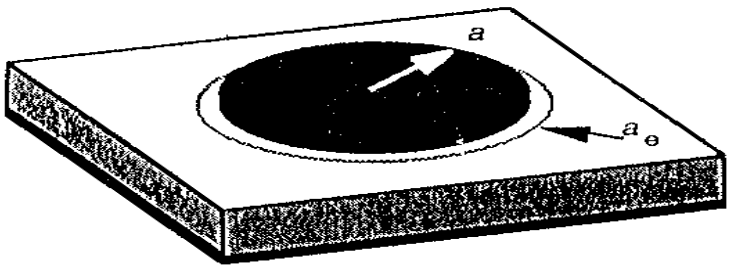

Figure2.7. Disk resonator and effective radius

When the substrate thickness is much smaller than the radius of the patch, the first modes of resonance are TM_{mno} modes, with resonant frequencies given by:

$$f_{mn} = \frac{c_o \chi_{mn}}{2p\, a_e \sqrt{\varepsilon_r}} \qquad (2.2)$$

Where χ_{mn} is the m^{th} extremum of the Bessel function J_n. The effective radius a_e and the unloaded quality factor Q_o for the fundamental TM_{110} mode are evaluated respectively, as[7]:

$$a_e = a\sqrt{1+\frac{2h}{\pi a}\ln(\frac{\pi a}{2h}+1.7726)} \quad (2.3)$$

$$Q_O = [(\lambda R_m / \pi Z_o \lambda) + \tan\delta]^{-1} \quad (2.4)$$

Where $\lambda = c_o/f$ is the free space wavelength,

$R_m = \sqrt{\omega\mu/2\sigma}$ Is the metal resistance, and

$Z_O = 120\pi\ \Omega$ is the free space impedance. This expression includes metal losses and dielectric losses but does not take into account radiation losses.

2.6. Microstrip Antenna Feeds

There are many configurations that can be used to feed microstrip antennas. The four most popular are the microstrip line, coaxial probe, aperture coupling and proximity coupling [1]. These are displayed in Fig.2.8. One set of equivalent circuits for each one of these is shown in Fig.2.9. The microstrip line is also a conducting strip, usually of much smaller width compared to the patch. The microstrip line feed is easy to fabricate, simple to match by controlling the inset position and rather simple to model. However, as the substrate thickness increases surface waves and spurious feed radiation increase, which for practical designs limit the bandwidth (2-5percent) [1].

Coaxial-line feed, where the inner conductor of the coax is attached to the radiating patch while the outer conductor is connected to the ground plane, are also widely used. The coaxial probe feed is also easy to fabricate and match, and it has low spurious radiation. For these above advantages, the coaxial feed type is selected in this thesis. However, there are some drawbacks in applying this feeding technique, such as it has narrower bandwidth and it is more difficult to model, especially for thick substrates ($h > 0.02\lambda_o$)[1]. Both the microstrip feed line and the probes possess inherent asymmetries, which generate higher order modes, which produce cross-polarized radiation. To overcome some of these problems non-contacting aperture coupling feeds, as shown in Fig.2.8.c have been introduced. The aperture coupling is the most difficult of all four to fabricate

and it also has narrow bandwidth. However, it is somewhat easier to model and has moderate spurious radiation. The aperture coupling consists of two substrates separated by a ground plane. On the bottom side of the lower substrate there is a microstrip feed line whose energy is coupled to the patch through a slot on the ground plane separating the two substrates. This arrangement allows independent optimization of the feed mechanism and the radiating element. Typically a high dielectric material is used for the bottom substrate, and thick low dielectric constant material for the top substrate. The ground plane between the substrates also isolates the feed from the radiating element and minimizes interference of spurious radiation for pattern formation and polarization purity for this design.The substrate electrical parameters, feed line width and slot size and position can be used to optimize the design. Typically matching is performed by controlling the width of the feed line and the length of the slot.

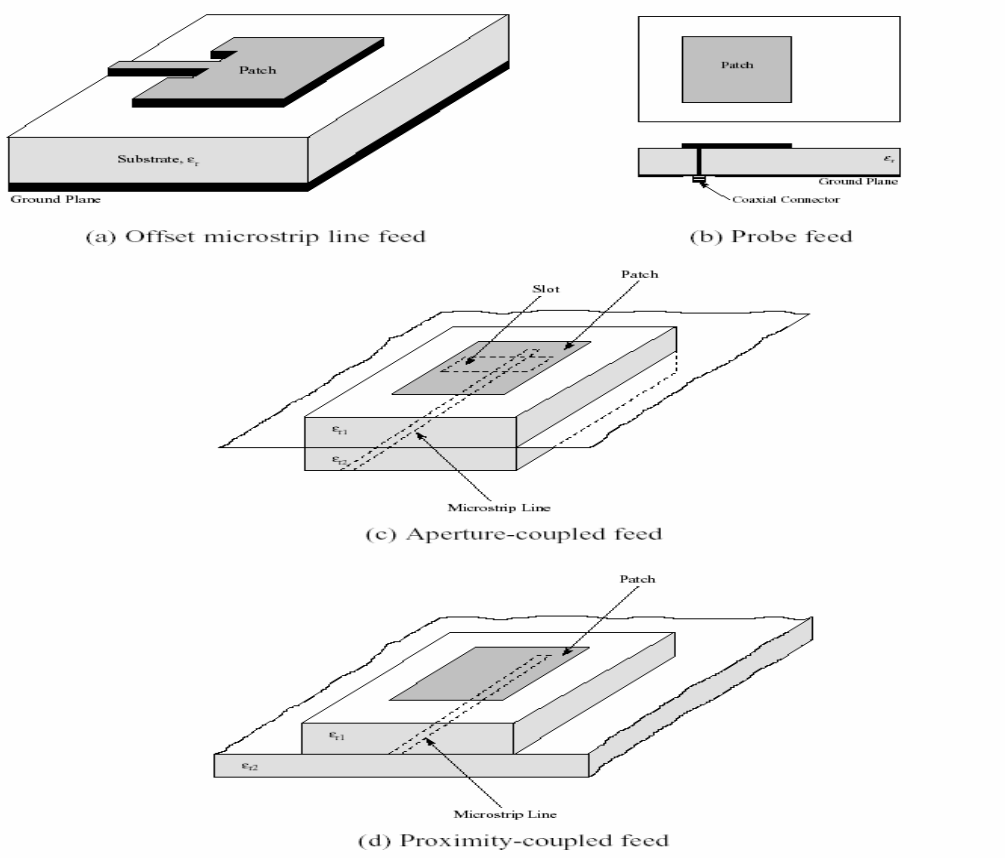

Figure2.8. Typical Feeds for Microstrip Antennas [1]

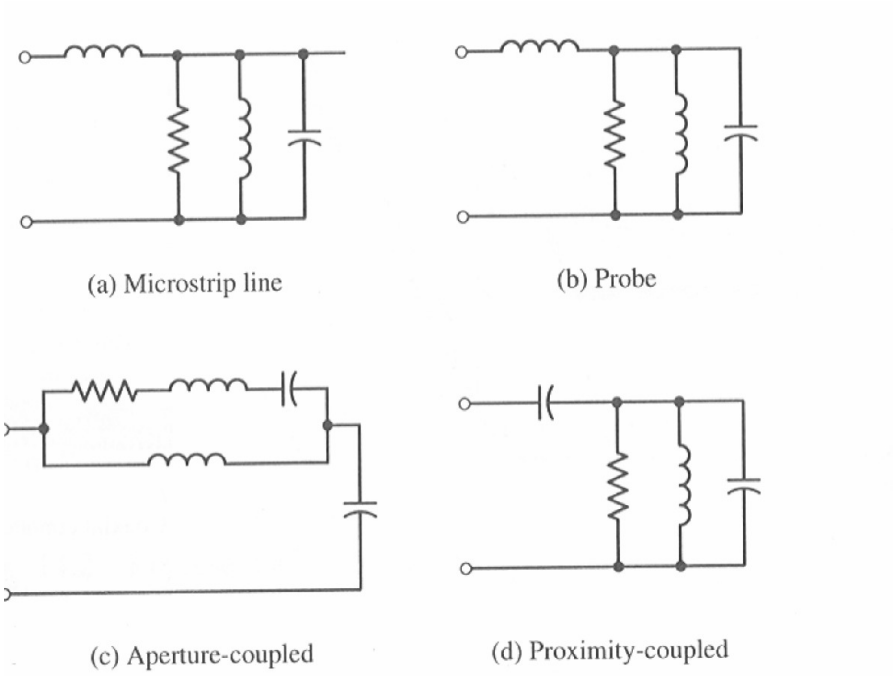

Figure2.9. Equivalent Circuits for Typical Feeds of Figure 2.8 [1]

2.7. Microstrip Antenna Feed Models

The two most common ways of feeding a microstrip antenna are by use of a coaxial probe feed and a microstripline feed. In the cavity model both of these sources are modeled essentially the same way. They are modeled by z-directed surface currents as illustrated in Fig.2.10. For a coaxial feed the current is assumed to flow uniformly over a cylinder of a diameter equal to that of the feed probe. For a microstripline feed the current is assumed to flow uniformly over a strip of width equal to that of the Stripline.

Simplified circuit model for a microstrip element is shown in the Fig.2.11 below. One can view that the input impedance of the element as the sum of a resonant component plus a feed-reactive component,

i.e. $Z_{in}=Z_{res}+jX_f$ (2.5)

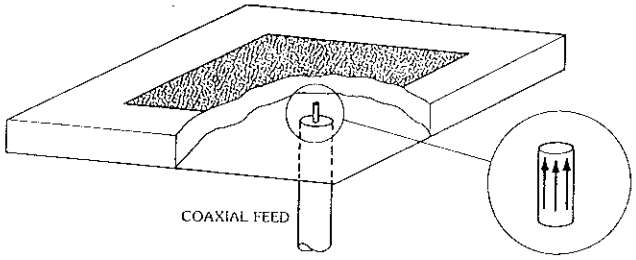

Figure2.10.Coaxially fed element and the simplified model obtained by removing the probe feed, closing the aperture of the coaxial cable, and impressing a uniform electric surface current on the surface corresponding the surface of the feed probe [13]

This decomposition of the impedance into resonant and nonresonant parts has been found quite useful in explaining the behavior of loaded elements

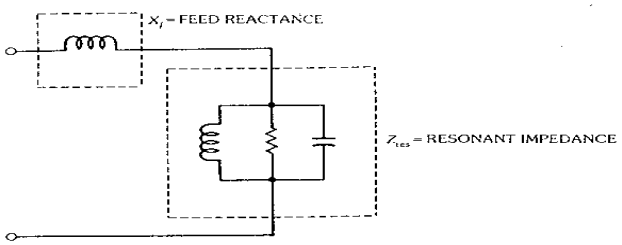

Figure2.11. Simplified Circuit Model of Microstrip Element valid over the band of a single, isolated mode [13]

In conclusion a typical plot of the resonant resistance and reactance versus frequency is shown by the solid and dotted curves in Fig.2.12. Near the resonant frequency of the (M, N) th mode the resistance reaches its peak value, denoted as R_{res} . This peak resistance does not occur exactly at the resonant frequency of the antenna, as can be seen from the figure, because of the presence of the feed reactance

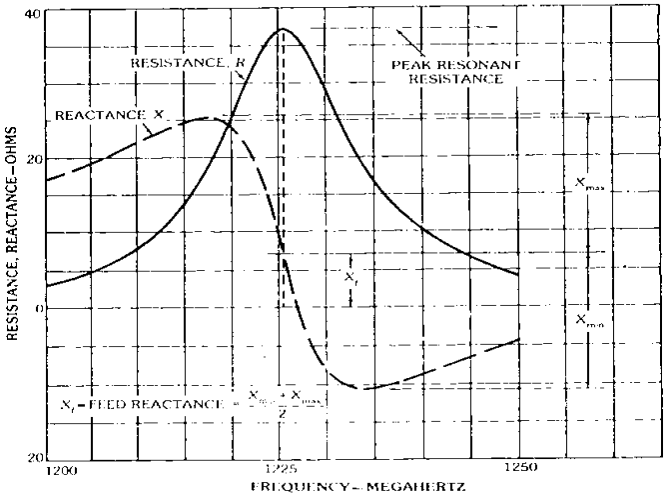

Figure2.12 Typical measured variation of resistance and reactance versus frequency in a 7.62-x11.43-x16-cm microstrip antenna illustrating one way to empirically determine the feed reactance [13]

2.8. Microstrip Antenna Models

Microstrip patch antennas have been analyzed using a variety of techniques. Three well-known methods are the transmission-line model, the cavity model, and full-wave numerical models. Below an overview of each of the methods are provided and the strengths and weaknesses of each will be discussed.

2.8.1. Transmission Line Model

The transmission-line model is the simplest of the three techniques and, as a result, is the least accurate. The microstrip antenna is modeled as two radiating slots that are separated by a distance L_{eff}. Referring to Fig.2.13.a, one can see the physical meaning of L_{eff}. It is essentially the length of the patch, L, plus an additional length $2\Delta L$, to account for the fact that the patch looks electrically wider due to the fringing fields. Balanis provides the following formula for the added length [1].

$$\Delta L = 0.412h\frac{(\varepsilon_{reff} + 0.3)(\frac{w}{h} + 0.264)}{(\varepsilon_{reff} - 0.258)(\frac{w}{h} + 0.8)} \tag{2.6}$$

In the above equation, ε_{reff} is the effective dielectric constant of a microstrip transmission line given by:

$$\varepsilon_{erff} = \frac{\varepsilon_1 + 1}{2} + \frac{\varepsilon_r - 1}{2}\left[1+12\frac{h}{w}\right]^{-1/2} \tag{2.7}$$

And, for an efficient radiator, a practical width that leads to a good radiation efficiency is

$$W = \frac{1}{2f_r\sqrt{\mu_o\varepsilon_o}}\sqrt{\frac{2}{\varepsilon_r+1}} = \frac{c}{2f_r}\sqrt{\frac{2}{\varepsilon_r+1}} \tag{2.8}$$

Thus the effective distance separating the two radiating slots becomes

$$L_{eff} = L+2\Delta L \tag{2.9}$$

Finally, Balanis uses this adjusted length to calculate the resonant frequency of the antenna [1]:

$$(f_r)_{100} = \frac{c}{2L_{eff}\sqrt{\varepsilon_{reff}}} \tag{2.10}$$

where, c is the speed of light in free-space.

Since the transmission-line model accounts for the fringing effects at the edges of the patch, it provides a good characterization of the resonant frequency. It also models input impedance of the antenna fairly accurately. However, it doesn't account for the effects of a truncated dielectric substrate or a finite ground plane nor does it provide insight into the radiation patterns of the antenna. Additionally, the model breaks down as the height of the dielectric substrate, h, becomes a significant portion of a wavelength [1].

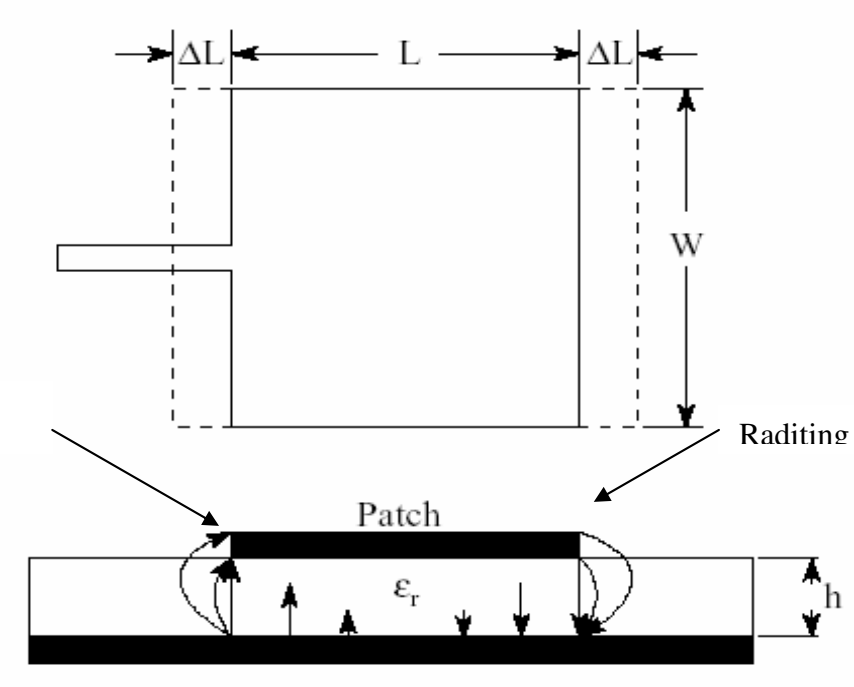

(a)

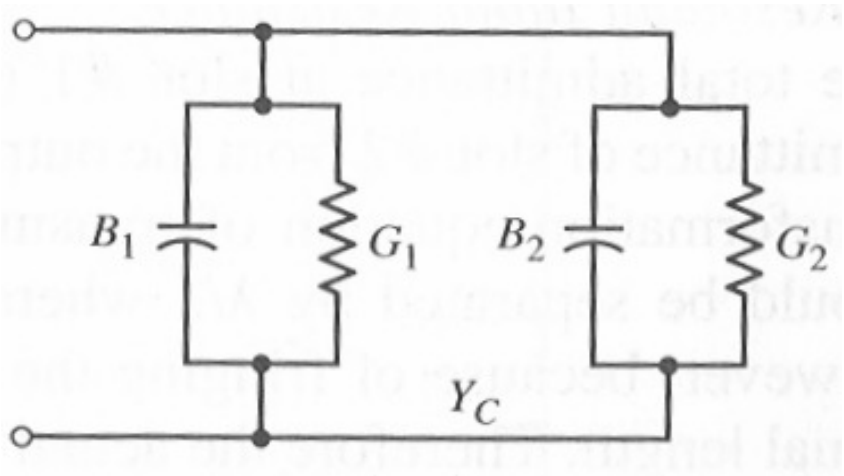

(b)

Figure2.13 (a) Transmission-line Model of a Microstrip Antenna (b) Equivalent Circuit Model.

As can be seen in the figure above each radiating slot is represented by a parallel equivalent admittance Y (with conductance G and susceptance B). The slots are labeled

as #1 and #2. The equivalent admittance of slot #1, based on an infinitely wide, uniform slot as derived in [1] is given by:

$$Y_1=G_1+JB_1 \qquad (2.11)$$

where for a slot of finite width W

$$G_1 = \frac{W}{120\lambda_O}\left[1-\frac{1}{24}(k_O h)^2\right] \qquad h'0.1\lambda o \qquad (2.12)$$

$$B_1 = \frac{W}{120\lambda_O}\left[1-.636\ln(k_o h)\right] \qquad h'0.1\lambda o \qquad (2.13)$$

Since slot #2 is identical to slot #1,its equivalent admittance is

$$Y_2=Y_1, \qquad G_2=G_1, \qquad B_2=B_1 \qquad (2.14)$$

The conductance of a single slot can also be obtained by using the field expression derived by the cavity model. In general the conductance is defined as

$$G_1 = \frac{2P_{rad}}{|V_o|^2} \qquad (2.15)$$

After some mathematical manipulations the asymptotic values are given as [1]:

$$G_1 = \begin{cases} \frac{1}{90}\left(\frac{W}{\lambda_0}\right)^2 & W \ll \lambda_0 \\ \frac{1}{120}\left(\frac{W}{\lambda_0}\right) & W \gg \lambda_0 \end{cases} \qquad (2.16)$$

The resonant input resistance can be seen as follows. The total admittance at slot #1(input admittance) is obtained by transferring the admittance of slot #2 from the output terminals using the admittance transformation equation of transmission lines. Ideally ,the two slots should be separated by λ/2 where λ is the wavelength in the dielectric substrate. However, because of fringing the length of the patch is electrically longer than the actual length. Therefore, the actual separation of the two slots is slightly less than λ/2. If the reduction of the length is properly chosen (typically 0.48λ′L′0.49λ)[1], the transformed admittance of slot #2 becomes

$$\bar{Y}_2 = \bar{G}_2 + jB_2 = G_1 - jB_1 \qquad (2.17)$$

Therefore the total input admittance is real and is given by

$$Y_{in}=Y_1+\bar{Y}_2=2G_1 \qquad (2.18)$$

Since the total input admittance is real, the resonant input impedance is also real, or

$$Z_{in}=1/Y_{in}=R_{in}=1/2G_1 \quad (2.19)$$

2.8.2. The Cavity Model

In order to gain insight into the radiating mechanism of an antenna, we need to first understand the near field quantities that are present on the structure. The cavity model aids in this regard since it provides a mathematical solution for the electric and magnetic fields of a microstrip antenna. It does so by using a dielectrically loaded cavity to represent the antenna. As we can see in Fig.2.14, this technique models the substrate material, but it assumes that the material is truncated at the edges of the patch. The patch and ground plane are represented with perfect electric conductors and the edges of the substrate are modeled with perfectly conducting magnetic walls. It should be noted that the cavity model does not include feed effects. The feed is shown in the figure for reference.

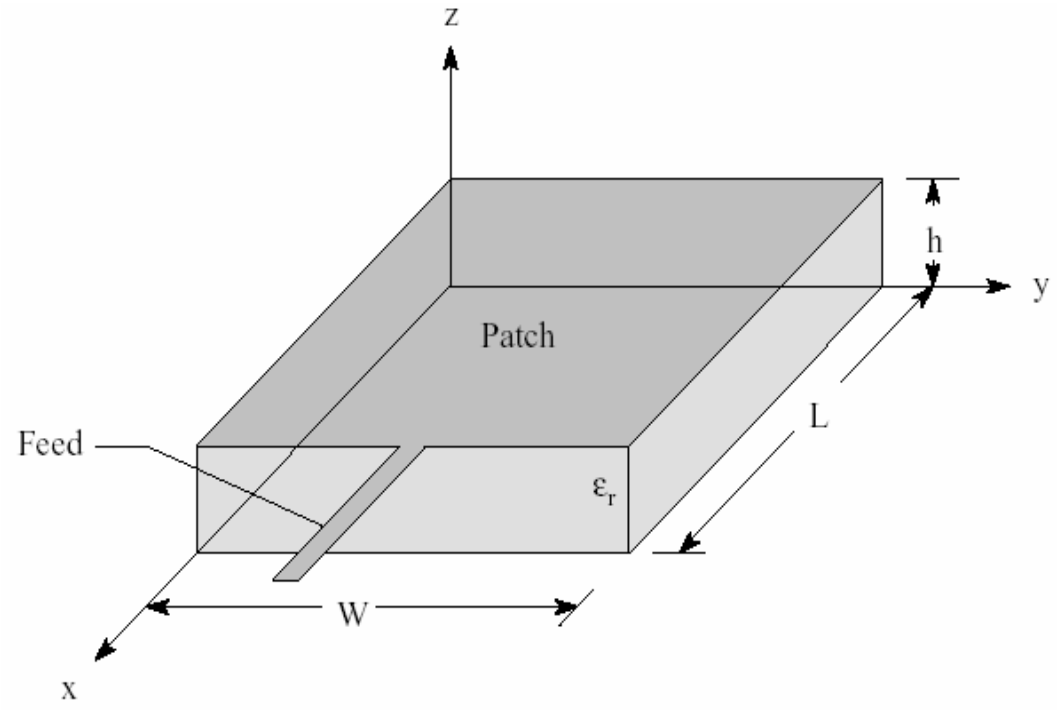

Figure 2.14 Geometry of Cavity Model

Balanis formulates a solution to the above cavity problem using the vector potential approach [1]. Summarizing the technique, we begin by assuming that the dielectric is very thin, which means that the electric field is constant along the height of the substrate, h, and is nearly normal to the surface of the patch. Therefore, we only need to consider

T_{mz} modes inside the cavity. Now, we can write an expression for the electric and magnetic fields within the cavity in terms of the vector potential A_z [1]:

$$E_X = -j\frac{1}{\omega\mu\varepsilon}\frac{\partial^2 A_Z}{\partial x \partial y} \qquad H_X = \frac{1}{\mu}\frac{\partial A_Z}{\partial y} \tag{2.20}$$

$$E_y = -j\frac{1}{\omega\mu\varepsilon}\frac{\partial^2 A_Z}{\partial Y \partial X} \qquad H_Y = \frac{1}{\mu}\frac{\partial A_Z}{\partial X} \tag{2.21}$$

$$H_z = -J\frac{1}{\omega\mu\varepsilon}\left(\frac{\partial^2}{\partial z^2} + k^2\right)A_z \qquad H_z=0 \tag{2.22}$$

Since the vector potential satisfies the homogenous wave equation:

$$\nabla^2 A_z + k^2 A_z = 0 \tag{2.23}$$

We can use separation of variables to write the following general solution.

$$A_z = [A_1\cos(k_x x) + B_1\sin(k_x x)][A_2\cos(k_y y) + B_2\sin(k_y y)][A_3\cos(k_z z) + B_3\sin(k_z z)]$$

Where k_x, k_y, and k_z are wave numbers. Applying the boundary conditions

E_x=0; for 0≤X≤L, 0≤y≤w, z=0;

And, 0≤x≤L, 0≤y≤W, z=h

H_x=0; for 0≤X≤L, y=0, 0≤z≤h

and 0≤x≤L, y=w, 0≤z≤h

H_y=0; for x=0, 0≤y≤ w , 0≤z≤h;

and x=L,0≤y≤w,0≤z≤h

We obtain a solution for the electric and magnetic fields inside the cavity as follows.

$$E_x = -j\frac{k_x k_z}{\varpi\mu\varepsilon} A_{mnp} \sin(k_x x)\cos(k_y y)\sin(k_z z)$$

$$E_y = -j\frac{k_y k_z}{\varpi\mu\varepsilon} A_{mnp} \cos(k_x x)\sin(k_y y)\sin(k_z z)$$

$$E_z = -j\frac{\left(k^2 - k_z^2\right)}{\varpi\mu\varepsilon} A_{mnp} \cos(k_x x)\cos(k_y y)\cos(k_z z)$$

$$H_x = -\frac{k_y}{\mu} A_{mnp} \cos(k_x x)\sin(k_y y)\cos(k_z z) \qquad (2.24)$$

$$H_y = \frac{k_x}{\mu} A_{mnp} \sin(k_x x)\cos(k_y y)\cos(k_z z)$$

$$H_z = 0$$

here,

$$k_x = \frac{m\pi}{L}, m = 0,1,2.....$$

$$k_y = \frac{n\pi}{W}, n = 0,1,2.....$$

$$k_z = \frac{p\pi}{h}, p = 0,1,2.....$$

in all the above cases, m=n=p ≠ 0

and A_{mnp} is the amplitude coefficient. Finally, the resonant frequencies for the cavity are given by [1]

$$\left(f_r\right)_{mnp} = \frac{1}{2\pi\sqrt{\mu\varepsilon}}\sqrt{\left(\left(\frac{m\pi}{L}\right)^2 + \left(\frac{n\pi}{W}\right)^2 + \left(\frac{p\pi}{h}\right)^2\right)} \qquad (2.25)$$

Examining the above field equations for $(T_{mz})_{100}$ dominant mode excitation, we see that $k_y = k_z = 0$ and the field components reduce to

$$E_z = -j\varpi A_{100}\cos\left(\frac{\pi}{L}x\right) \qquad (2.26)$$

$$H_y = \frac{\pi}{\mu L} A_{100} \cos\left(\frac{\pi}{L} x\right) \tag{2.27}$$

We can convert to equivalent electric and magnetic current densities using:

$$\vec{J} = \hat{n} \times \vec{H} \tag{2.28}$$

$$\vec{M} = -\hat{n} \times \vec{E} \tag{2.29}$$

where n is the outward directed surface normal. The magnetic field is zero along the x =0 and x=L walls and is normal to the surface along the y=0 and y=w walls. Therefore, no equivalent electric current density flows on the walls of the cavity. The electric field results in a non-zero magnetic current density on the walls of the cavity. Fig.2.15 shows both the electric field and corresponding magnetic current densities for the microstrip antenna. The magnetic currents can be broken into a pair of radiating slots and pair of non-radiating slots. The radiating slots are in phase so they will constructively interfere in the far field. Thus, these two slots form the primary radiating mechanism for the microstrip antenna. On the other hand, the non-radiating slots are out of phase so they will destructively interfere in the far field and will not contribute to the radiated fields.

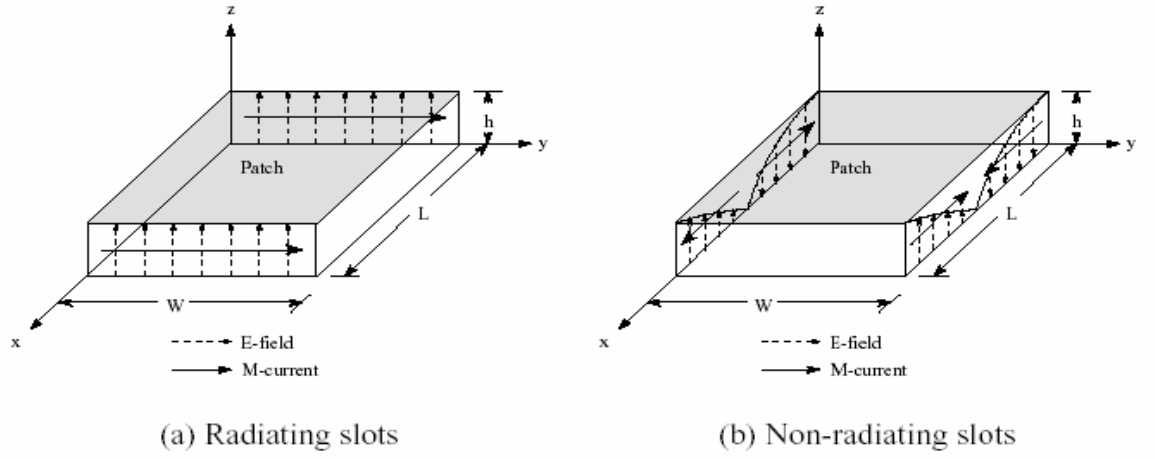

Figure 2.15. Field Configuration and Current Densities for Microstrip Patch [13]

From the above results, we can see that the cavity model provides an excellent insight into the radiating mechanism of a microstrip patch antenna. It provides the field configurations of the radiating and non-radiating slots that can be used to solve for the radiations patterns. Since the antenna is modeled as a cavity, additional work is necessary

to accurately model the input impedance. An effective loss tangent needs to be added to account for the power that is lost to radiation. Alternately, the radiated energy can be modeled using an impedance boundary condition at the walls.

Although, the cavity model is quite adept at modeling the radiating mechanisms for a microstrip patch antenna, it does have some limitations. First, it does not take the feed effects in to consideration. Nor does it model the adverse effects introduced by a finite substrate and ground plane. Therefore, one way to combat these limitations is just to apply numerical techniques.

2.8.3. Full-wave Numerical Models

In some cases, we may need to understand how the behaviors of an antenna are affected by its surroundings. For example, we may want to develop a model that includes the effects of feed structures, a finite ground plane, or a case enclosure. For problems, such as these, the techniques described above are highly impractical. Fortunately, there are a variety of numerical analysis techniques that can handle these problems quite nicely, including the Method of Moments (MOM), the Finite-Element Method (FEM), and the Finite Difference Time Domain (FDTD) method. All three of these analysis techniques are computationally intensive, which in the past, due to lack of high performance machines (both in speed and memory capacity), limited the size and complexity of problems that could be approached. However due to recent advances in computing capabilities, these techniques have became much more applicable to higher problems. In addition, these techniques are somewhat generalized so they are capable of modeling a variety of antenna types. The details of each technique are intricate, so we will focus on the FDTD method because the simulation software used in this thesis is the field solver EMPIRE.

The FDTD method uses a discretization in time and space to calculate a solution of Maxwell's curl equations directly in time domain [9]:

$$\nabla \times \vec{E} = -\mu \frac{\partial \vec{H}}{\partial t} \tag{2.30}$$

$$\nabla \times \vec{H} = \varepsilon \frac{\partial \vec{E}}{\partial t} + \vec{J} \tag{2.31}$$

Rearranging these equations, with

$$\vec{J} = \sigma \vec{E} \tag{2.32}$$

We obtain:

$$\frac{\partial \vec{H}}{\partial t} = -\frac{1}{\mu} \nabla \times \vec{E} \tag{2.33}$$

$$\frac{\partial \vec{E}}{\partial t} = \frac{1}{\varepsilon} \nabla \times \vec{H} - \frac{\sigma}{\varepsilon} \vec{E} \tag{2.34}$$

Evaluating the vector curl operator (∇xA) and employing central differencing in both time and space to approximate the partier derivatives, one can obtain six update equations (one for each component of the electric and magnetic fields).

For example, the update equation for the E_x component is as follows [9]:

$$E_x^n(i,j,k) = \left[\frac{\varepsilon}{\varepsilon + \sigma \Delta t}\right] E_x^{n-1}(i,j,k) + \left[\frac{\Delta t}{\varepsilon + \sigma \Delta t}\right] \cdot \left[\begin{array}{l} \dfrac{H_z^{n-1/2}(i,j,k) - H_z^{n-1/2}(i,j-1,k)}{\Delta y} \\ -\dfrac{H_y^{n-1/2}(i,j,k) - H_y^{n-1/2}(i,j,k-1)}{\Delta z} \end{array}\right] \tag{2.35}$$

The electromagnetic structure is modeled by approximating its geometry and composition with Yee cells of different material parameters (both conductivity and relative dielectric constant). Fig.2.16 depicts an example of Yee cell along with its corresponding field calculation points. At the outer boundaries of the computational space an absorbing boundary condition is used to simulate free-space radiation. In order to avoid numerical instabilities in the finite-difference algorithm, the time increment must not violate the courant stability condition [9]:

$$\Delta t \le \frac{(\mu\varepsilon)^{1/2}}{\left[\dfrac{1}{\Delta x^2} + \dfrac{1}{\Delta y^2} + \dfrac{1}{\Delta z^2}\right]^{1/2}} \tag{2.36}$$

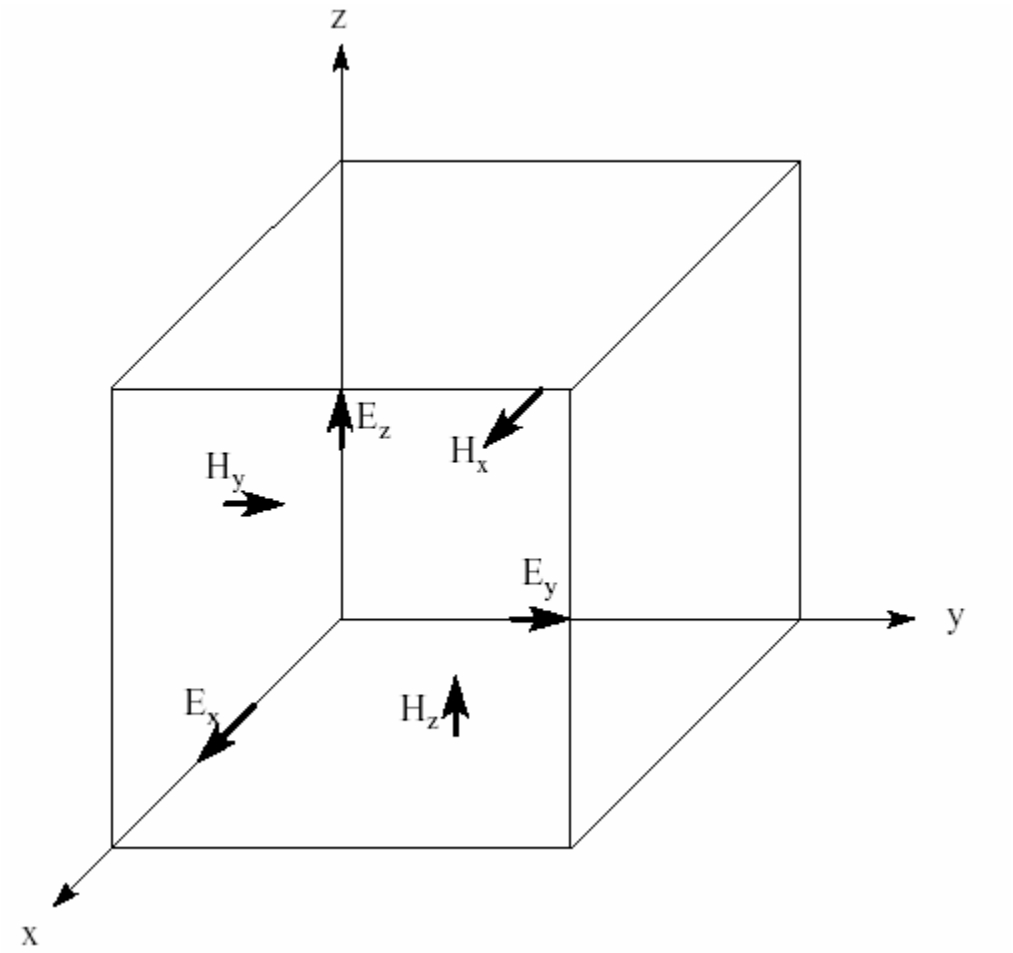

Figure 2.16.Example of a Yee cell with Field Calculation Points [9]

An excitation is then applied to the computational model and E and H field computations are alternately matched through time from time zero to the desired stopping point. Results can be viewed either in time domain or in frequency domain. In order to obtain frequency characteristics of the antenna, it is necessary to compute a Fast-Fourier Transform (FFT) of the transient output data.

The FDTD techniques presented above allow antennas to be modeled in fine detail. Feed lines, ground planes, and case enclosures can all be included in the computational model. In addition, the techniques are highly generalized so a member of antennas can be analyzed.

2.9. Microstrip Antenna Efficiency

For a microstrip antenna, efficiency is defined as the power radiated divided by the power received by the input to the element. Factors that reduce efficiency are the dielectric loss, the conductor loss, the reflected power (VSWR), the cross-polarized loss, and the power

dissipated in any loads involved in the elements. Most microstrip antennas are between 80 and 99 percent efficient. For very thin elements the Q of the microstrip cavity becomes so high that the current losses become excessive, and the thickness becomes so small that the conductance across the cavity yields excessive dielectric losses. This usually occurs when the thickness is reduced to about λ_o /1000.At this thickness, the resonance VSWR can be matched to 50 Ω, but the very narrow bandwidth leads to temperature instabilities; that is, a slight change in temperature causes the VSWR to rise rapidly, and the reflection losses reduce efficiency.

Dielectric losses are eliminated by using air as a substrate. Since most of these elements have large separation between the element and the ground plane, the Q is also reduced and so are conductor and VSWR losses. Most of these elements have efficiency of 95 to 99 percent. Air loaded elements are usually built as separate entities and are not photoetched in large arrays. Also the radiating element needs support. A single metal part, or bolt is used at the center of the element for support. Even though, the former method can help supporting an air-loaded patch, here in this thesis use of a very thin dielectric substrate and air in between the patch and the ground plane and apply the concept of suspended dielectric substrates to find the effective dielectric constant of the whole system.

Antenna "efficiency" is different than antenna "Gain". Antenna efficiency quantifies the resistive loss of the antenna in terms of the proportion of power that is actually radiated versus the power that is first delivered to it. Antenna gain, however, is a directional quantity that refers to the signal that can be derived from an antenna relative to a reference dipole.

2.9.1. The Model

Fig.2.17 illustrates an antenna loss model in which a resistor is placed in series with the radiation resistance. Since the model includes no reactance, there is an implicit assumption that the measurements must be taken at resonance. The equations to be derived later require this assumption.

Antenna efficiency is calculated according to equation 2.32 (the derivation of which is described in Appendix A):

$$\eta = \frac{P_{rad}}{P_{in}} = \frac{P_{rad}}{P_{rad} + P_{loss}} = \frac{R_{rad}}{R_{rad} + R_{loss}} \tag{2.37}$$

Where:η=Antenna efficiency (%)

P_{rad}=Radiated power (W)

P_{in}=Total power available to the antenna (W)

P_{loss}=Power loss due to resistive loss (W)

R_{rad}=Radiated equivalent resistance (Ω)

R_{loss}=Equivalent loss resistance (Ω)

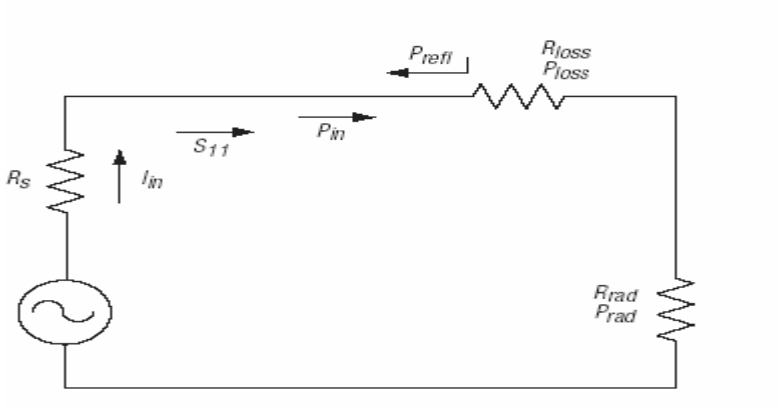

Figure 2.17. Antenna Loss Model

It doesn't matter if the antenna is matched to the source resistance, R_s or not. While it is desirable and necessary to match the antenna in actual case, the match is not part of the problem of finding the resistance ratio expressed in the above equation. Therefore, the radiated power only needs to be related to the power transferred forward at the point shown in Fig.2.17. If the resistances (R_{loss} and R_{rad}) can be effectively separated by measurement, antenna efficiency can be calculated.

Chapter 3

Single Band Microstrip Patch Antenna Design and Results

3.1. Introduction

In this chapter, the procedure for designing a rectangular microstrip patch antenna is explained. Then, a compact rectangular microstrip patch antenna is designed for use in cellular phones and simulations are performed. Finally, the results obtained from the simulations are discussed.

3.2. Design specifications

The three essential parameters for the design of a rectangular microstrip patch antenna are:

1. Frequency of Operation (f_r): the resonant frequency of the antenna must be selected appropriately. The Global Systems for Mobile communications (GSM) uses the frequency range from 890-960 MHz [8]. Hence the antenna designed must be able to operate in this frequency range. The resonant frequency selected for this design is 930 MHz.

2. Dielectric Constant of the Substrate (ε_r): the dielectric material applied for this design has a dielectric constant of 4.4. Use of a substrate with a high dielectric constant can reduce the dimensions of the antenna. However, for the radiation modes most used such substrates result in elements, which are electrically small in terms of free-space wavelengths and consequently have relatively smaller bandwidths and low efficiencies.

3. Height of dielectric substrate (h): for the microstrip patch antenna to be used in cellular phones, it is essential that the antenna is not bulky. Hence, the height of the dielectric substrate selected here is 7mm.

The essential parameters of the design are: **f_r= 0.93GHz, ε_r= 4.4,and h = 7mm.**

3.3. Design Procedure:

The design of a low profile, wide-band multiband patch antenna is very complicated. The fact is that the lowest antenna profile, the widest impedance bandwidth and the most omni-directional (lowest ripple level) azimuth plane radiation pattern cannot be achieved simultaneously [14]. Fig.3.1 below shows the conventional rectangular microstrip patch antenna, which is presented here for the sake of easy analysis and design of practical microstrip antennas for mobile handsets.

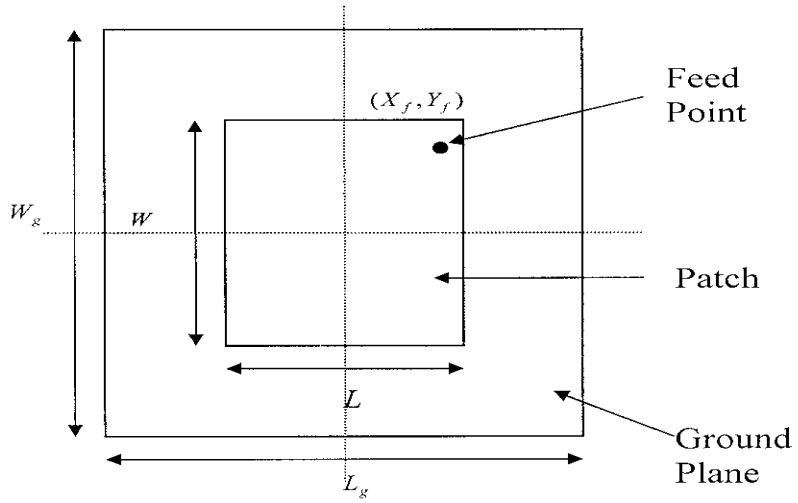

Figure 3.1. Top View of Microstrip Patch Antenna

The transmission line model described in chapter two will be used to design the antenna.

Step 1. Calculation of the width (W): the width of the microstrip patch antenna is given by equation (2.8) as [1]:

$$W = \frac{c}{2f_r}\sqrt{\frac{2}{(\varepsilon_r + 1)}} \tag{3.1}$$

Substituting c=3e8m/s, ™_r=4.4 and f_o=930MHz.we get **W=98.16mm**

Step 2: Calculation of effective dielectric constant (™_{reff}):

Equation (2.7) gives the effective dielectric constant as [1]:

$$\varepsilon_{reff} = \frac{\varepsilon_r + 1}{2} + \frac{\varepsilon_r - 1}{2}\left[1 + 12\frac{h}{W}\right]^{-1/2} \tag{3.2}$$

Substituting, ™_r=4.4,W=98.16mm and h=7mm we get **™_{reff}=3.95**

Step 3: Calculation of the effective length (L_{eff}): equation (2.9) gives the effective length as [1]:

$$L_{eff} = \frac{c}{2f_r\sqrt{\varepsilon_{eff}}} \tag{3.3}$$

Substituting, ™_{reff}=3.95,c=3e8m/s, f_o=930MHz, we get **L_{eff}=81.2mm**

Step 4: Calculation of the length extension (ΔL): equation (2.6) gives the length extension as [1]:

$$\Delta L = 0.412h \frac{\left(\varepsilon_{reff} + 0.3\right)\left(\frac{W}{h} + 0.264\right)}{\left(\varepsilon_{reff} - 0.258\right)\left(\frac{W}{h} + 0.8\right)} \quad (3.4)$$

Substituting, ™$_{reff}$=3.95, W=98.16mm, and h=7mm,we get **ΔL=3.251mm**

Step 5: Calculation of the actual length of the patch (L): the actual length is obtained by subtracting the length extension from the effective length as:

$$L = L_{eff} - 2\Delta L \quad (3.5)$$

Substituting L_{eff}= 81.2mm and ΔL = 3.251mm we get **L = 74.698 mm**

Step 6: Calculation of the ground plane dimensions (L_g and W_g)

The transmission line model is applicable to infinite ground planes only. However, for practical considerations, it is essential to have a finite ground plane. It has been shown in many open literatures that similar results for finite and infinite ground planes can be obtained if the size of the ground plane is greater than the patch dimensions by approximately six times the substrate thickness all around the periphery. Hence, for this design, the ground plane dimensions would be given as:

$$L_g = 6h + L = 6 \text{ x}7 \text{ mm} + 74.698\text{mm} = 116.698\text{mm} \quad (3.6)$$

$$W_g = 6h + W = 6\text{x } 7 \text{ mm} + 98.16\text{mm} = 140.16\text{mm} \quad (3.7)$$

Step 7: Determination of feed point location (x_f, y_f):

A coaxial probe type feed is to be used in this design. As shown in Figure 3.1, the center of the patch is taken as the origin and the feed point location is given by the coordinates (x_f, y_f) from the origin. The feed point must be located at that point on the patch, where the input impedance is 50 Ohms for resonant frequency.

As can be seen from the above calculations to find the antenna size, the dimensions are large to be practically applied in cellular phones. Therefore, to achieve a smaller antenna size, we need to short circuit the radiating patch to the antenna's ground plane with a shorting pin and utilize an asymmetric branch line slit to meander the excited patch surface currents in the top patch, which leads to a large reduction in the required top patch dimensions. The ground plane dimension is modified to fit into the PCB dimensions of most handsets ($40\times80\text{mm}^2$). Figure 3.2 below shows the modified top patch design to achieve the 900MHz operation.

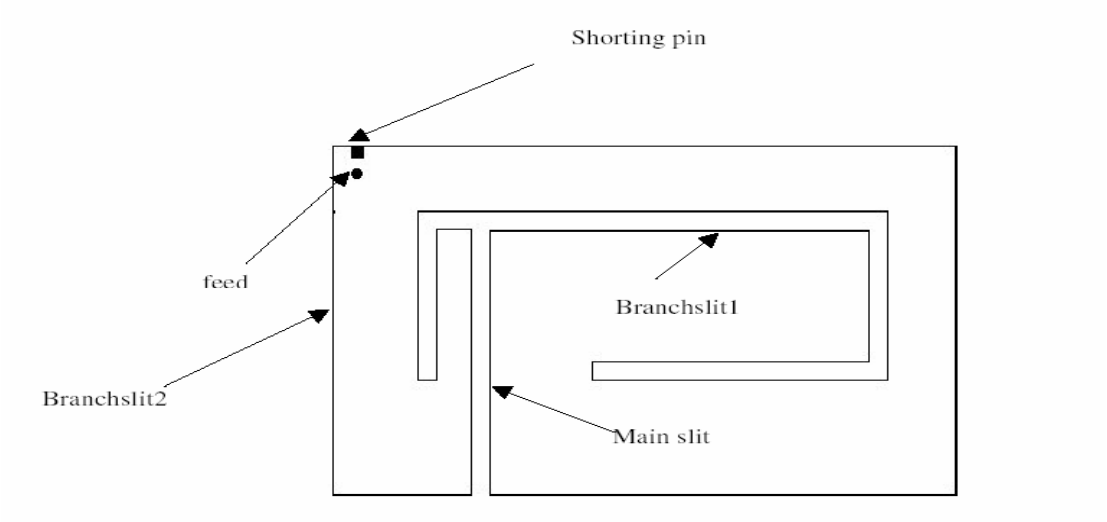

Figure 3.2 Geometry of the Proposed Antenna

Fig.3.2 above uses a single resonant path for the desired operation. The design utilizes an asymmetric branch-line slit to meander the excited patch surface currents in the top patch, which leads to a large reduction in the required top patch dimensions of the patch, and the first resonant frequency of the meandered resonant path is tuned to fall in the range of frequencies for 900 MHz operations. It should also be noted that the wavelength of the first resonant frequency in this design corresponds to about 4 times the length of the meandered patch surface current path, starting from the feed point to the portion of the patch encircled by the long folded branch slit. That is, this meandered patch portion is operated as a radiator with resonant length of about 0.25 wavelengths.

Fig.3.3.below shows the three-dimensional view of the simulated antenna structure, which helps us for easy visualization of the whole arrangement.

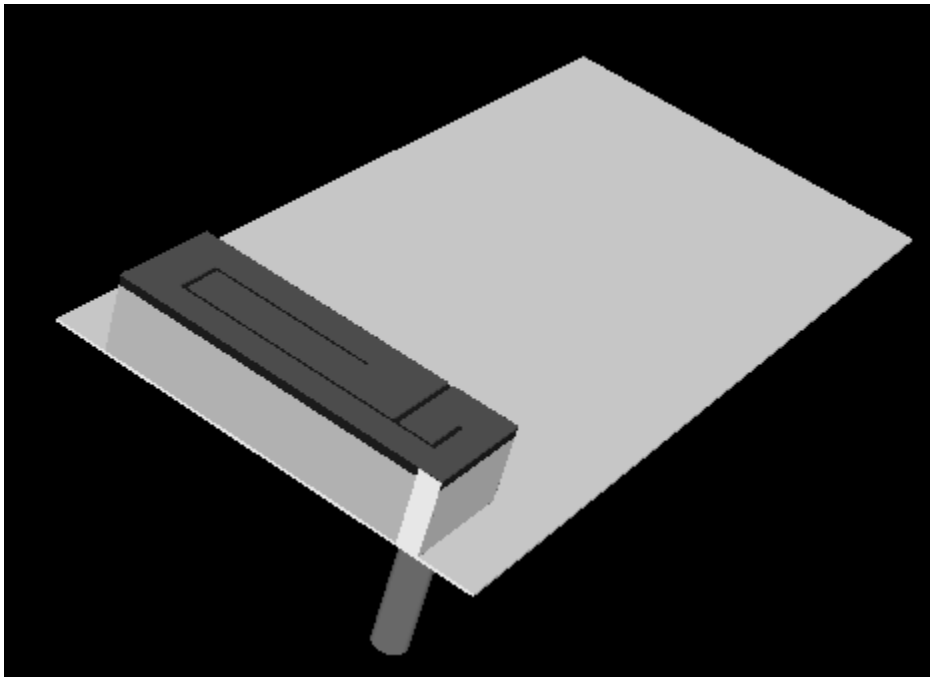

Figure3.3 Simulation Model of the Structure

In Fig.3.3 above, the top patch is mounted on a dielectric substrate of relative dielectric constant 4.4.The substrate has a thickness of 0.8-mm. The remaining thickness is left to be filled with air. This design uses the same analysis as that of suspended microstrip lines where air and another dielectric substrate are used simultaneously in between the ground plane and the top patch. Therefore, the whole structure (that is, the dielectric substrate plus air) can be analyzed the same way as suspended microstrips. By using very thin dielectric substrates of low dielectric constant, the dielectric loss can be minimized.

Fig.3.4 below shows the suspended microstrip line, whose analysis can be helpful for the case at hand [10].

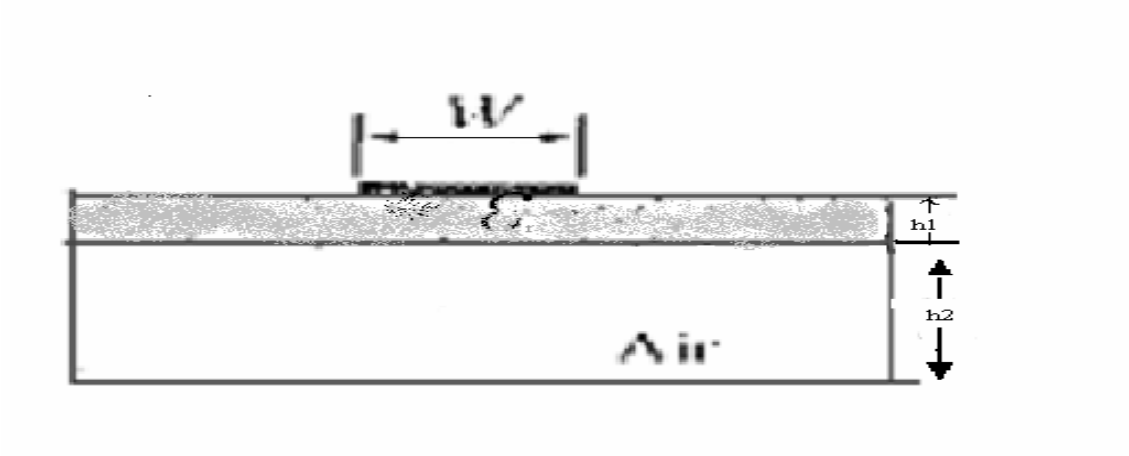

Figure 3.4 Suspended Microstrip Line

The closed form expression for the effective dielectric constant of the substrate explained in previous chapter may be modified to find the effective dielectric constant of the above type structures as [10]:

$$\sqrt{\varepsilon_{reff}} = \left[1+\frac{h1}{h2}\left(a-b\ln\left(\frac{W}{h2}\right)\right)\left(\frac{1}{\sqrt{\varepsilon r}}-1\right)\right]^{-1} \tag{3.8}$$

Where $$a = \left[0.8621 - 0.1251 \ln \frac{h_1}{h_2}\right]^4 \tag{3.9}$$

$$b = \left[0.4986-0.1397\ln\frac{h1}{h2}\right]^4 \tag{3.10}$$

The accuracy of the above equation for the calculation of the effective dielectric constant is within 1 percent over the ranges $1[W/h_2[8,0.2[h_1/h_2[1$, and $\varepsilon_r[6$ [10].

For example in this design the relative permittivity for the dielectric is selected as 4.4. Therefore the effective dielectric constant of the whole structure is given by:

$$\sqrt{\varepsilon_{reff}} = \left[1+\frac{h1}{h2}\left(a-b\ln\left(\frac{W}{h2}\right)\right)\left(\frac{1}{\sqrt{\varepsilon r}}-1\right)\right]^{-1} \tag{3.11}$$

Where $$a = \left[0.8621-0.1251\ln\frac{h_1}{h_2}\right]^4 \tag{3.12}$$

$$=[0.8621-0.1251\ln(0.8/6.2)]^4$$

$$=1.564$$

$$b = \left[0.4986 - 0.1397 \ln \frac{h1}{h2}\right]^4 \qquad (3.13)$$

$$= [0.4986\text{-}0.1397\ln(0.8/6.2)]^{4}$$

$$=0.379$$

Therefore, after substituting all the parameters in equation (3.11), one obtains $\boldsymbol{\varepsilon_{reff}=1.22.}$

As the calculation above shows, the effective dielectric constant is nearly equal to unity. This is preferred because air (or space) has the lowest loss, and makes the patch element full size, which gives maximum gain. This all arrangement of substrates is required to get proper height for the design (that is 7-mm), since the height of the patch above the ground plane should be approximately two percent of the width of the patch. With air dielectric a half wave square patch should be a minimum of 0.001wavelengths above the ground plane. Lower heights result in higher Q and high currents resulted in higher losses.

A branch line slit consisting of a main slit, a long folded branch slit (branch slit 1 in Fig.3.2), and a short bent branch slit (branch slit 2 in the Fig.3.2) is embedded on the top patch. The main slit, which has an open end at the patch boundary, and the long folded branch slit in the top patch are mainly for effectively meandering the excited patch surface current paths. On the other hand, the short bent branch slit is mainly for achieving enhanced impedance matching for the excited resonant frequencies to obtain wider operating bandwidths. As can be seen, the required length of the short bent branch slit is much smaller than that of the long folded branch slit. The feed point is located close to the shorting plate and both the feed point and the shorting plate are also required to be placed at the patch edge near the short bent branch slit. In this case, a large meandering of the patch encircled by the long folded branch slit can be obtained. This large meandering leads to a large reduction in the required patch dimensions for the desired band of operation.

As can be clearly seen, the length of the meandered patch surface current path corresponds to half of the wavelength at 1800MHz operation. Therefore, if properly tuned, this meandered patch can function as a dual band antenna.

3.4. Simulations Setup and Results

3.4.1. General

The software used to model and simulate the microstrip patch antenna is the Finite Difference Time Domain (FDTD) method based field solver EMPIRE by IMST GmbH. EMPIRE is a full-wave electromagnetic simulator based on the finite-difference method, which means that the two Maxwell's curl equations are discretized in space and time [9]. This is accomplished by mapping the structure of interest onto a rectangular grid where the unknown field components are located in each cell. Because, the two maxwell's curl equations are the governing equations, which are functions of both space and time, the FDTD based field solver Empire is selected. It analyzes three-dimensional and multi layer structure of general shapes. It can be widely used in the design of Microwave Integrated Circuits (MICs), Radio Frequency Integrated Circuits (RFlCs), patch antennas, wire antennas, and other radio frequency (RF)/wireless antennas. It can be used to calculate and plot the input return loss, input impedance, current distributions as well as the radiation characteristics [9].

Because of the nature of the electromagnetic problem, an initial value problem has to be solved. This means that the unknown field for a certain time is calculated from the field values before. The FDTD method employs an efficient time stepping algorithm, known as the Yee's leapfrog scheme [?], which will be explained in Appendix B, to solve the initial value problem. The size of the time steps is related to the size of the grid for stability reasons and cannot, therefore, be defined independently. So the definition of a suitable grid is an important task for efficient simulation.

The duration of a simulation run is proportional to the number of time steps needed. It strongly depends on the quality factor of the systems, which cannot easily be determined. In certain cases, even instabilities can occur before reaching the steady state.

Due to the limited memory resource of a computer, only a finite number of cells can be processed. Therefore, the calculation area has to be terminated with boundary conditions.

Most of the problems encountered in analyzing and designing high frequency elements are due to the unknown electromagnetic field behavior. Often these problems are called "parasitics" or "coupling effects". The reason for the inability to predict the electromagnetic field behavior is that Maxwell's equations cannot be solved analytically

for any practical structure (with the exception of some academic examples). Therefore, one often has to deal with approximations, which have limitations in applicability.

3.4.2. Simulation Setup and Results

In the numerical analysis of this antenna the FDTD based simulation software explained above is used, because it is simple to understand and can be used to analyze antennas of complex structures. As the detailed theory on FDTD method is available from Yee [9], only a brief outline will be presented here. The first steps in designing an antenna with an FDTD code is to grid up the object. A number of parameters must be considered for the software to work successfully .The grid size must be small enough so that the fields are sampled sufficiently to ensure accuracy.

A Gaussian pulse voltage with unit amplitude, given by

$$V(t)=\exp\left[-(t-t_o)^2/T^2\right], \tag{3.14}$$

Where T denotes the period and t_o identify the center time, is excited in the probe feed.

After the final time domain results are obtained, the current and voltage are transformed to those in the Fourier domain. The input impedance of the antenna is then obtained from

$$Z_{in}=V(f)/I(f) \tag{3.15}$$

The results of input impedance are then used to obtain the return loss characteristics of the antenna, from which the operating bandwidths can easily be deduced. To get the radiation pattern characteristics, a sinusoidal excitation at the probe feed is used, which is given by

$$V(t)=\sin(2\pi f_r t), \tag{3.16}$$

Where f_r denotes the resonant frequency of interest. The field distributions are recorded at one instant of time after the steady state has been reached. After the field distribution has been obtained, the radiation pattern can be readily calculated by using the near field to far-field transformation.

Figure3.5. below shows the voltage waveforms at the input terminals of the antenna. The main waveforms helping the analysis are the incident voltage and the reflected voltage.

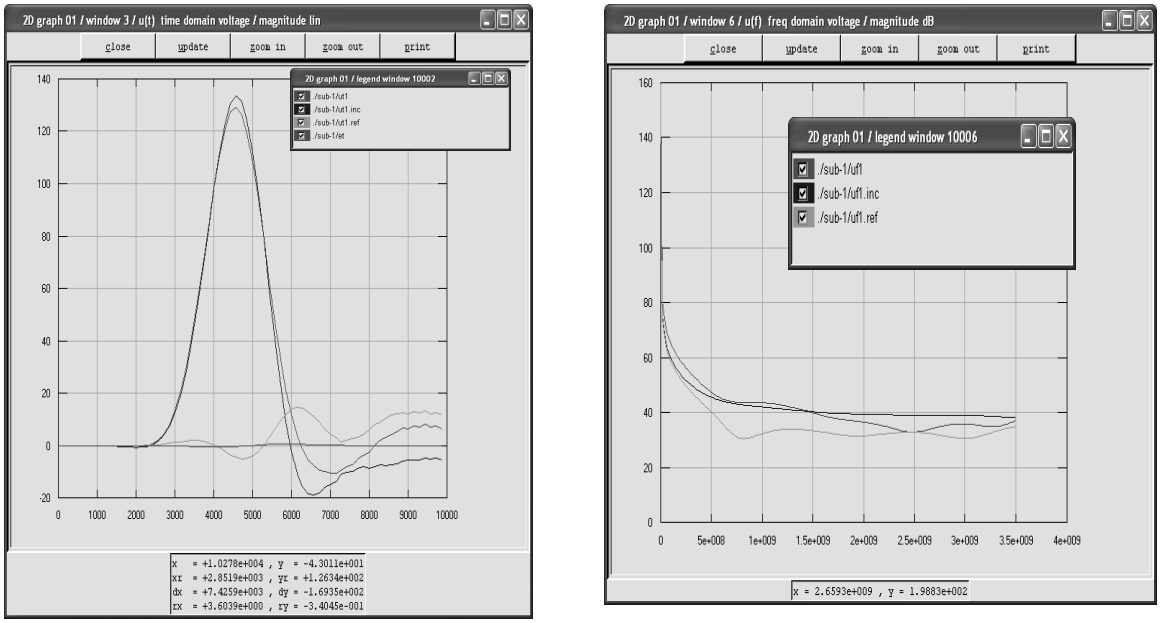

(a) (b)

Figure3.5 Voltage Waveforms seen at the Input terminal of the Antenna (a) as a function of time steps, (b) as a function of frequency

As can be seen from the legend in Fig3.5, the reflected voltage amplitude has small amplitude over a range of time steps especially where the antenna is expected to radiate. This implies that much of the energy applied at the input is radiated and a small amount is reflected back. Since the antenna is a one-port network, it is clear that much of the energy is radiated in to space if it is not reflected back. As the above snap shows the incident voltage amplitude is always greater than the reflected voltage amplitude. One also can easily observe that at the operating frequency for which the antenna is designed, the reflected voltage amplitude is the lowest. This can be taken as a good justification that the antenna functions well at the designed frequency.

3.4.3. Return loss and Antenna Bandwidth

Fig.3.6 below shows simulation model of the antenna structure in two dimensions.

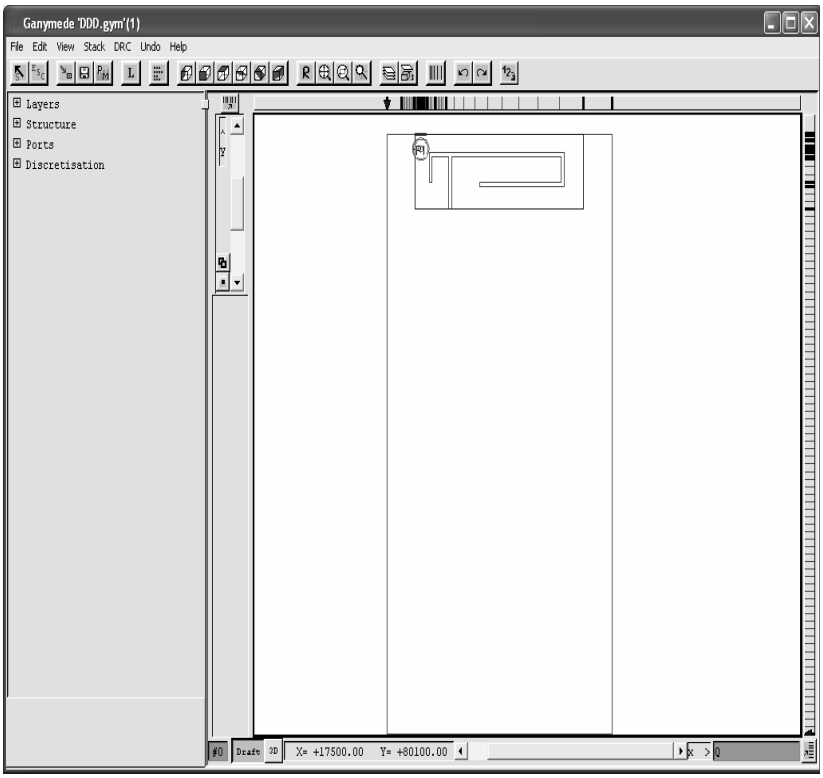

Figure 3.6. Simulation Model of the Structure

The coaxial probe feed used is designed to have a radius of 0.4mm. The center frequency is selected as the one at which the return loss is minimum. As described in chapter two, the bandwidth can be calculated from the return loss (RL) plot. The bandwidth of the antenna is said to be those range of frequencies over which the return loss is greater than 7.3-dB, which is equivalent to 2.5:1 VSWR. The bandwidth of the antenna for this feed point location is seen to be 45-MHz and a center frequency of 830-MHz is obtained which is very close to the desired frequency of operation. It was observed from many trials of simulations that as the feed point location is moved away from the edge of the patch, the center frequency starts to decrease. This may be due to the highly sensitive nature of the input impedance bandwidth to position of the probe. Figure 3.7 below shows the return loss snap taken during simulation. The return loss (in dB) is plotted as a function frequency.

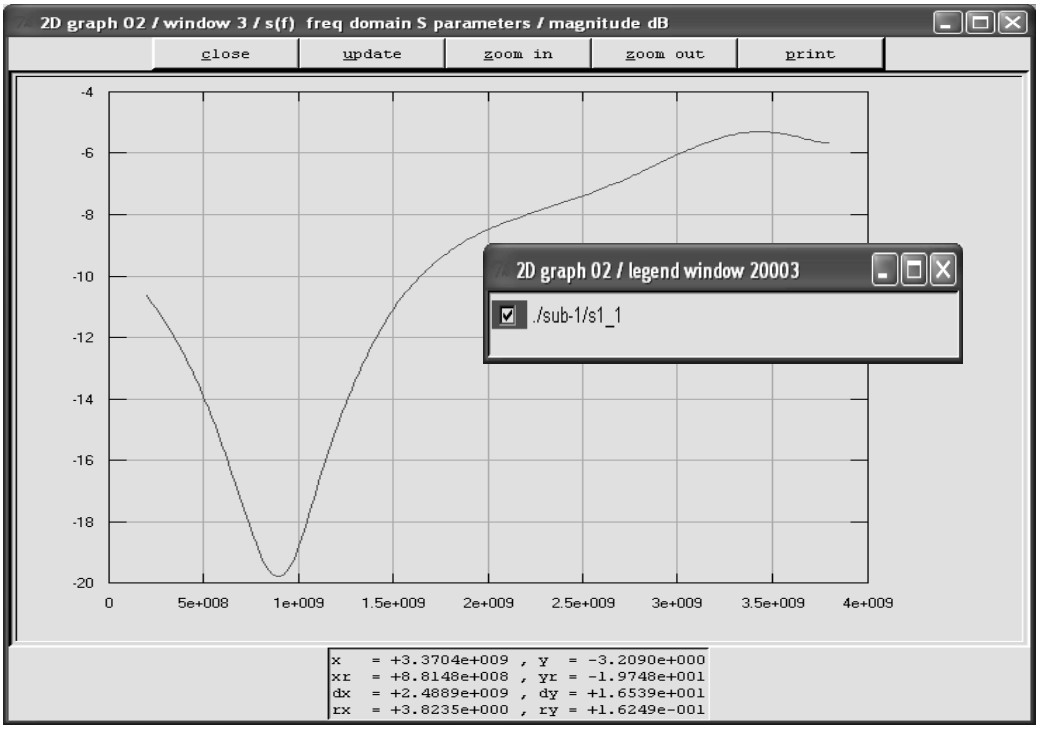

Figure 3.7: Return Loss for Feed at the edge of the patch

Although the designed antenna has a much smaller antenna volume of only 30 x 10x 7 mm^3, it should be noted that the obtained bandwidth is still not large enough to meet the bandwidth requirement of the GSM band [70MHz(890–960MHz)][8]. Further enhancement in the impedance bandwidth is required to obtain optimal performance of the GSM mobile phones.

3.4.4. Input Impedance

As has been stated in Chapter two, we expect pure real impedance at frequencies where the patch resonates, that is, where the patch is designed to radiate. As a result, the input impedance plot in Fig 3.8 below roughly shows, around the desired radiating frequency, sufficient reactance cancellation can only occur inside a narrow bandwidth. In addition, one needs to match the resonant resistance with the characteristic impedance of the feed line. A small antenna can be tuned to resonate with an appropriate addition of reactance, or it can be made to self-resonate so that the reactance cancellation at resonance happens naturally in the antenna structure. Since adding external reactance for this purpose increases the power loss and it also requires extra space, it is advisable to follow the second alternative.

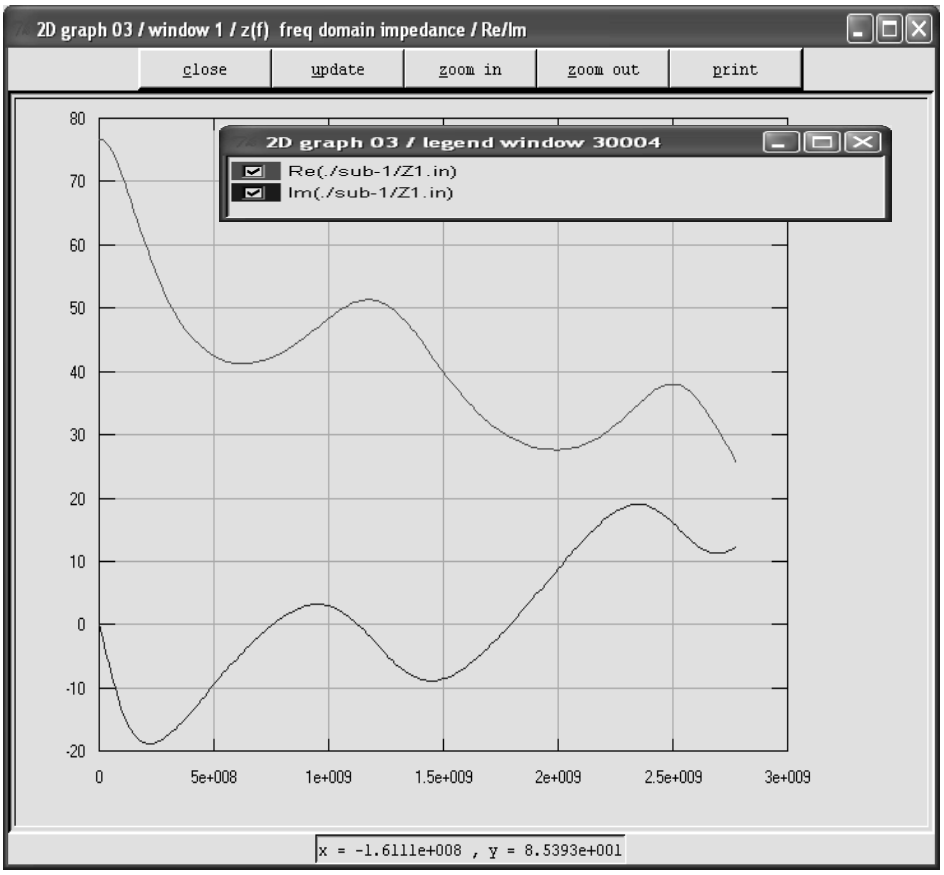

Fig3.8.Input Impedance Plot

As can be seen from the above simulation output for the input impedance, the peak of the real part of the impedance does not occur exactly at the resonant frequency of the antenna, this is because of the presence of the feed reactance, which cannot be eliminated.

3.4.5. Radiation Pattern Plots

A microstrip patch antenna radiates normal to its patch surface. The elevation pattern for ϕ=0 and ϕ=90 degrees would be important. Figure3.9 below show the 2D radiation pattern of the antenna at the designed frequency for ϕ=0 and ϕ=90 degrees.

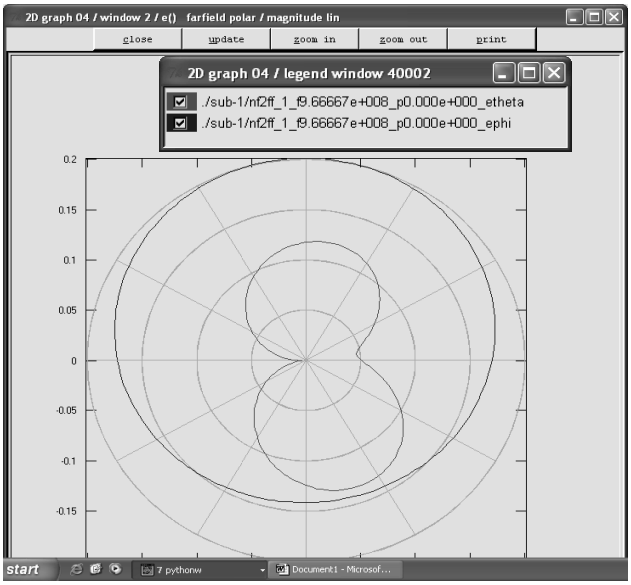

Figure3.9: Elevation Pattern for ϕ=0 and ϕ= 90 degrees

The maximum gain is obtained in the broad side direction. Figure 3.10 below shows the snap taken from the animation of the three dimensional radiation pattern of the simulated antenna for GSM900 band.

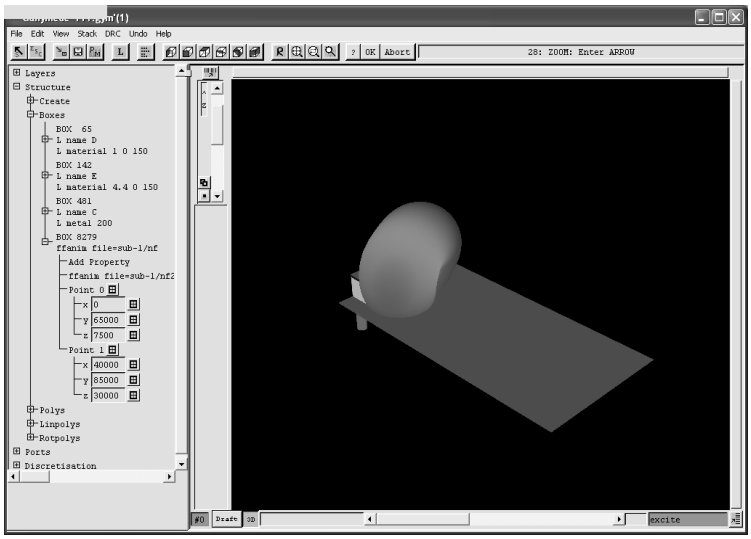

Figure3.10 Radiation Pattern of the Simulated Antenna for GSM900

As can be seen from the above simulation out put the pattern clearly shows that the antenna radiates most of the energy on the patch side and there is a small amount of radiated energy on the back side. This is another desired advantage of planar antennas over the conventional whip antennas, which shows omnidirectional radiation. This

suggests that the possible electromagnetic energy absorption by the users head can be reduced. As the above simulated radiation pattern in Fig3.10 shows us, when the microstrip antenna designed is placed into a cellular phone, its orientation would be such that, the patch side should be placed away from the user's head.

In conclusion, it can be seen from the simulation results that, the antenna performs well at the operating frequency. There is also some deviation from the theoretically expected operating frequency, the main reason for this is the discretization applied during simulation. Also from the radiation pattern seen above, maximum of the energy radiated is away from the user's head, which guarantees that an acceptable level for the specific absorption rate by the user's head can be maintained. But as can be seen from the return loss snap taken from the simulation, one can see that the whole of the GSM900 band is not covered by the antenna bandwidth, therefore some work is needed to be done to tackle this.

Chapter 4

Multiband Internal Antennas for Mobile Handsets

4.1. Introduction

Current wireless communication systems utilize several different radio communication standards and separate at many different parts of the frequency spectrum. In this fractured service environment, terminals operating in multiple systems and frequency bands can offer a better service coverage than single band and single-system terminals. Multiband antennas are essential components of multiband terminals [8].

Generally, there seems to be an increasing trend in the number of radios in a mobile terminal, which translates into an increase in the number of antennas or antenna functions. Integrated antennas have become very popular due to the advantages they provide with respect to the aesthetical design of mobile phones. It has been shown in many papers that the maximum bandwidth of an antenna of a given size depends strongly on the dimensions of the mobile phone in which the antenna is installed. Multiband operation, which nowadays is almost a common standard, requires the use of enhanced radiating elements. Moreover, other aspects such as small size, weight, and integration have a great relevance for the final design, and material and assembling costs must be kept as low as possible. The preferred solution is the use of radiating patches with multiple resonances, covering different bands, which are easily adapted to the shape of the handset, and can therefore be integrated within the back cover [8]. This solution has a number of advantages: terminal designers can forget about the antenna when designing the external cover, the phone becomes more robust as there are no external radiating elements that could break off and the antennas can be produced in a more cost effective way.

Internal planar inverted-F antennas (PIFAs) are very suitable in such applications since they are compact, low profile and easy to manufacture [8]. However, several techniques applied simultaneously are necessary to reduce the size of these antennas while maintaining good multiband/wideband performances. Starting with the main quarter-wavelength element as shown in chapter three, these techniques are: addition of parasitic shorted patches, capacitive loads and slots on the resonators.

The designed antennas are expected to function properly in the GSM (global system for mobile communications, 890-960MHz), DCS (Digital Communication System, 1710-1880MHz), PCS (Personal Communication Services, 1850-1990MHz), and UMTS (Universal Mobile Telecommunication System, 1920-2170 MHz). A considerable number of antennas designed for mobile phones have been published recently, enough to be organized into a book [8]. In the following, a short overview of existing shorted microstrip patch antenna type internal multiband antennas and their design techniques is presented to illustrate the recent progress in the field.

4.2. General Realization Methods

For the promising radiating top patch designs for multiband operation, there are two major design concepts: one design uses different resonant paths to generate separate resonant modes for multiband operation, and the other uses the first few resonant frequencies of a single resonant path for the intended multiband operation. Now let us see each design concept in a little detail.

4.2.1. Separate Antenna Elements

Irrespective of the antenna type a multiband antenna can be constructed by combining two or more separate single band antenna elements. If a large isolation can be achieved between the antenna elements operating at different bands, they can be optimized nearly independently, which simplifies the design [8]. For example, Fig.4.1 below shows the top patch of a planar inverted–F antenna comprising two separate patches of different sizes for achieving 900MHz and 1800MHz operations. Note that the larger and smaller patches have separate shorting pins and are operated, respectively, in the 900 and 1800MHz bands as quarter–wavelength resonant structures.

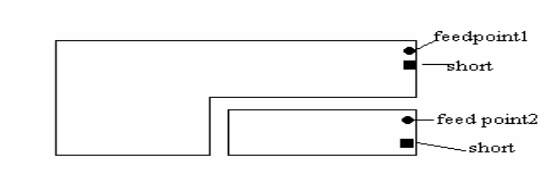

Figure 4.1.Top patch of the dual-frequency PIFA comprising two separate patches achieving 900 and 1800 MHz operations [8]

This version of dual-frequency operation utilizes dual feed design. The dual feed (feed point 1 for the larger patch and feed point 2 for the smaller patch) is also used in the design, which can find applications where mobile phones have receivers with dual front

ends. In addition to achieve a compact antenna size, a portion of the larger patch is removed to accommodate the smaller patch.

A triple frequency (that is, triple band) version applying the same design concept is shown below in Fig.4.2 below.

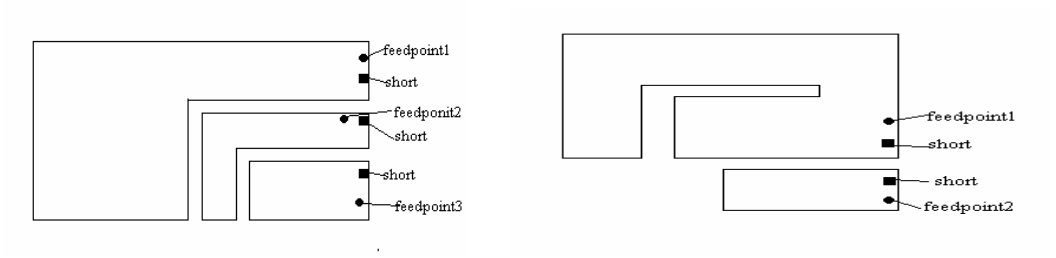

(a) (b)

Figure 4.2 Top patch of the triple-frequency PIFA comprising (a) three separate patches with a triple feed and (b) two separate patches with a dual feed for achieving 900,1800 and 2450 MHz operations [8]

As the figure shows, there are two promising configurations of the top patch of the triple frequency microstrip patch antenna for the 900, 1800, and 2450 MHz operations. In Figure 4.2.a, the top patch comprises three separate patches with a triple feed, patch 1 is for GSM operation in the 900 MHz band, patch 2 is for DCS operation in the 1800MHz band, and patch 3 is for WLAN operation in the 2450MHz band. Note also that, these three patches are arranged in a compact configuration and have separate shorting and feed points. These three patches are all operated as quarter-wavelength resonant structures. Such antenna design with a triple feed can find applications where mobile phones require separate feeds for operations in GSM, DCS and WLAN bands.

For the configuration shown in Figure4.2.b, the top patch consists of two separate patches, with the larger patch (patch 1 in the figure) loaded with an L-shaped slit for GSM and DCS dual frequency operations. In this design the smaller patch (patch 2) is for WLAN operation in the 2450 MHz band and is also operated as a quarter–wavelength resonant structure. The two patches utilize different shorting and feed points, and such a design is suitable for mobile phones using the same feed for GSM and DCS operations and a second feed for WLAN Operation.

4.2.2. Use of inductor and capacitor (LC) resonators

One possibility of realizing a dual band antenna, for example at 900 and 1800 MHz band operations is connecting two separate patch sections with a parallel LC resonator (as in Fig.4.3 below) to separate the radiating top patch into two subpatches of different sizes which provide two resonant paths of different lengths to achieve the 900/1800 MHz operation. That is, at resonance, the parallel resonator acts as an open circuit (large reactance) disconnecting the two patch sections, which produces the higher resonant frequency. At frequencies below its resonance, the parallel resonator acts as an inductive load connecting the two patch sections, which produces the lower resonant frequency.

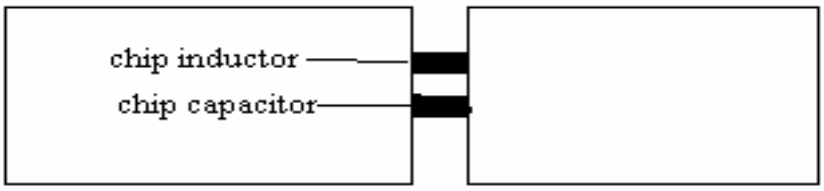

Figure4.3 Use of LC resonators to achieve dual band operation [8]

4.3. Single Element having two or more Resonances

Here, the major design consideration is to adjust the antenna's first few resonant frequencies at the desired radiating frequencies. To achieve this goal, the techniques of using a branch-line slit to achieve a lengthened resonant path, inserting several linear slits to meander the top patch, using a shorted spiral strip with various strip widths, folding a meandered top patch and so on have been successfully applied.

To include the WLAN operation in the 2.4GHz band, designs of triple-frequency PIFAs for operations in the 900,1800,2450 MHz bands have been reported, which include the use of two or three separate top patches, a meandered top patch, and a branch-line strip with a folded end. The techniques of using a parasitic shorted patch placed coplanar with the driven patch or stacked on top of the driven patch to enhance the operating bandwidth of the antenna have also been reported [8]. Now let us have a brief look at the different possibilities in designing the multiband antenna based on the above design procedure.

4.3.1 Patch with a U-shaped Slot

Recently, instead of using an L-shaped slit or a folded slit to obtain two separate sub patches in the radiating top patch, a design using an embedded U-shaped slot (figure 4.4), has been used. In this design, a smaller rectangular patch of dimensions L_2 x W_2 for operating in the 1800MHz band is obtained in the central portion of the original rectangular patch of dimensions L_1XW_1, which is for the 900MHz band operation. Because the smaller rectangular patch is embedded within the radiating top patch, it is also expected that this design can provide reduced electromagnetic wave power absorption by the user's head in the higher frequency band. The lower (f_1) and upper (f_2) operating frequencies of this planner antenna design can also be approximately determined from [8]:

$$f_1 \cong \frac{c}{4(l_1 + w_1)} \tag{4.1}$$

and

$$f_2 \cong \frac{c}{4(l_2 + w_2)} \tag{4.2}$$

The above two equations make the design of such a dual frequency PIFA easy to achieve, and c in the equations is the speed of light in free space.

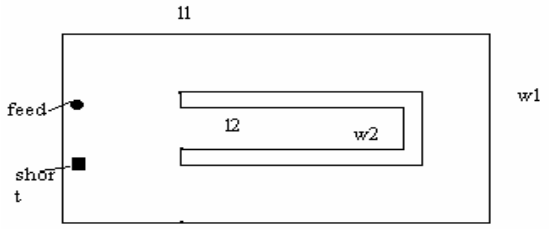

Figure4.4.Top patch of the Dual Frequency PIFA with an embedded U-slot [8]

4.3.2. Patch with an L-Shaped or Folded Slit

Fig. 4.5 shows two promising designs of the top patch of the dual frequency PIFA using a single probe feed and a common shorting pin. Fig.4.5.a, with the use of an L-shaped slit inserted at the patch boundary, the rectangular top patch can be separated into two sub patches of different sizes. The dimensions of the larger and the smaller sub patches can

be designed to roughly resonate as a quarter-wavelength structure to operate in the 900 and 1800 MHz bands respectively. Two sub patches can also be obtained by using a folded slit as shown in Fig.4.5.b. Note that, in this case, the resonant path provided by the smaller sub patch starts from the feed point and then extends into the center portion of the rectangular patch. A large portion of this resonant path is thus surrounded by the outer larger sub patch, which has the advantage of obtaining reduced backward radiation, leading to a smaller electromagnetic wave power absorption by the user's head in the 1800MHz band operation.

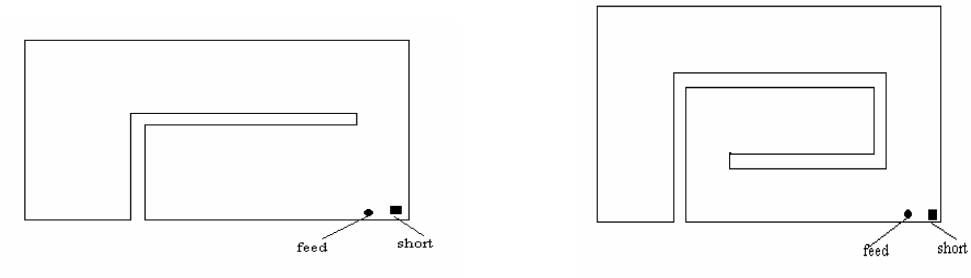

(a) (b)

Figure4.5 Top patches of the dual-frequency PIFA (a) an L-shaped slit and (b) a folded slit [8]

4.3.3. Patch with a Branch Line Slit.

This method of design aims to achieve a lengthened resonant path for the excited patch surface currents in the top patch, which leads to a large reduction in the required top patch dimensions of the antenna, and the first few resonant frequencies of the meandered resonant path are also tuned to obtain the desired ratio of the resonant frequencies.

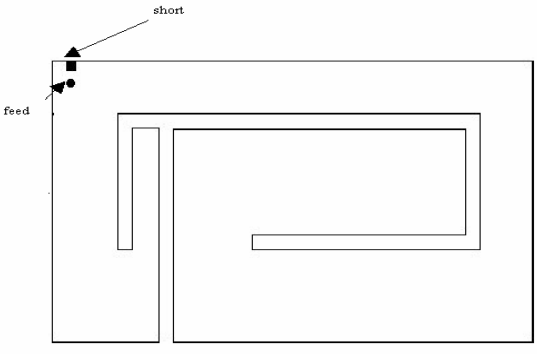

Figure4.6. Top patch of the antenna applying branch line slit [8]

4.3.4. Meandered Patch with/without a Parasitic Shorted Patch

By properly meandering the top patch of the antenna, the frequency ratio of the antenna's first two resonant frequencies can be tuned to be about 2.0, which makes it very promising for obtaining the 900 and 1800 MHz operations. [8] By further incorporating the use of a parasitic shorted patch, (see Figure 4.7 below) a much-enhanced bandwidth in the upper band of the PIFA has also been demonstrated [8]. In this design, the obtained impedance bandwidth, determined by 6-dB return loss (3:1 VSWR), reaches 535MHz in the upper band covering the required bandwidth of the DCS and PCS operations.

This relatively larger upper band bandwidth is mainly due to the added parasitic shorted patch, which introduces an additional resonant mode to the upper band and makes the upper band become a dual resonant band. This condition leads to an enhanced impedance bandwidth. In addition, this design has a sufficient bandwidth in the lower band (about 115MHz) to cover the required bandwidth in the GSM operation. In this case, the obtained PIFA design is suitable for applications in GSM/DCS/PCS triple-band mobile phones.

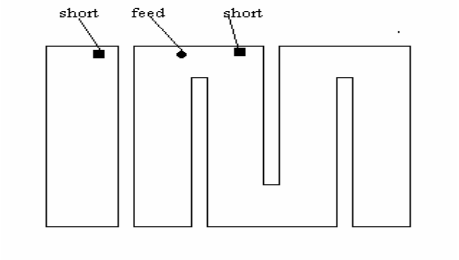

Figure 4.7. Top patch of the dual–frequency PIFA with a meandered patch and a parasitic shorted patch [8]

4.4. On the Design of Internal Multiband Antennas

The bandwidth and total efficiency of internal multiband antennas are limited by the total volume allowed for the antenna .The bandwidth-to-volume ratio can be increased by generating dual or multiple resonances at each band. If the bandwidth becomes larger than necessary, it can be traded off for smaller size or better matching and thus larger total efficiency. When the antenna size is small enough, even the use of known multiresonant techniques will not provide sufficient operation bandwidth.

One also needs to consider the operation of two bands, which are overlapping. There are two possible alternatives to achieve this: to excite a single mode with a sufficient

bandwidth, or excite two mutually coupled modes. If the latter strategy is chosen, it is essential to be able to perfectly control the coupling mechanism, since any, modification in the geometry of the patch can result in an important loss of bandwidth .The main concern is then how to tune one of the bands without interfering with the performance of the others

From the basic operation point of view, the excitation of resonances at desired frequencies is obviously important in the design of multiband antennas. Currently, however, the space allowed for internal handset antennas is so small that the resonant modes of the antenna elements alone cannot cover the necessary system bandwidths. Furthermore, it has been reported that for a frequency around 1.8GHz the maximum available bandwidth has a minimum for mobiles measuring around 100mm in length [8]. For this is a typical length for today's mobiles, it is obvious that new antenna concepts have to be investigated in order to meet the technical requirements of integrated multiband antennas for such mobiles.

As has been explained in the previous sections, multiband operation is almost a must nowadays. Therefore, the methods applicable to achieve these have their own advantages, application areas and drawbacks. After studying all the above methods of achieving multiband antennas, focus has been made in this thesis on the addition of a shorted parasitic patch to the main radiator. This has the provision of adding a third higher band. Applying this method, there is a small increase in the whole antenna dimension and this will be dealt with in the next chapter.

CHAPTER 5

Multiband Microstrip Patch Antenna Design and Simulation Results

5.1. Introduction

In this chapter, the procedure for designing the multiband microstrip patch antenna will be explained. The results obtained from the simulation are discussed.

5.2. Design procedure

As explained in chapter three, a 900-MHz microstrip patch antenna was designed. As has been shown in addition to the intended 900-MHz operation, the frequency ratio of the first two resonant frequencies can be adjusted to be about two, by fine-tuning the length of the meandered top patch of the PIFA. This makes the single band antenna very promising for obtaining the 900 and 1800-MHz operations (i.e. dual band operation). That is, this meandered patch portion can be operated as a radiator with resonant lengths of about 0.25 and 0.5 wavelengths. In the previous design, the length (l) of this meandered current path is about 83.3-mm. That is, the first or lower frequency for the proposed antenna has a wavelength corresponding to be about 4.0 times the length (l), and the second or upper frequency has a wavelength of about 2.0 times the length (l). By further incorporating the use of a parasitic shorted patch (see the geometry shown in Fig.4.7, a much-enhanced bandwidth in the upper band of the PIFA can be achieved [8]. That is, the experimentally studied antenna consists of a single shorted patch, which can function as a dual band radiator and a shorted patch is positioned next to the main radiator to obtain a doubly tuned resonance and a wider impedance bandwidth at the upper operating band. We next try to apply the above mentioned design methods in order to reach to the desired multiband operation.

5.3. Design Method

To achieve the multiband operation, we add a shorted parasitic patch positioned at the open slot of the main radiator. The parasitic patch is positioned to be electromagnetically coupled to the driven patch and participates in the radiating properties of the whole

element. For this to be achieved the gap between the driven element and the parasitic patch is optimized by using many trials of simulation.

Figure5.1 below shows the geometry of the resonant antenna under consideration. In this case, two resonant elements are used: one meandered metallic patch and one metallic strip, which are mounted on a single supporting FR4 substrate (thickness 0.6-mm and relative permittivity 4.4) and arranged in a compact configuration.

(a)

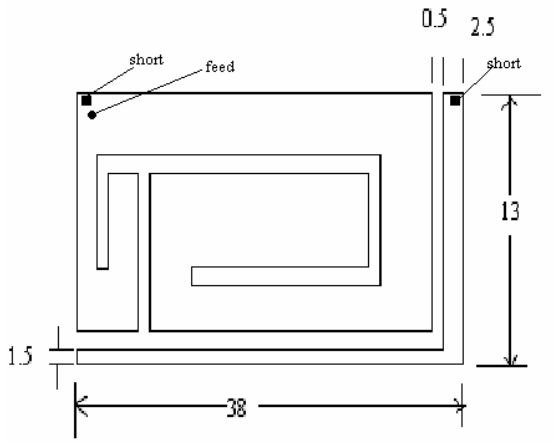

Note: all dimensions are in millimeter (mm).

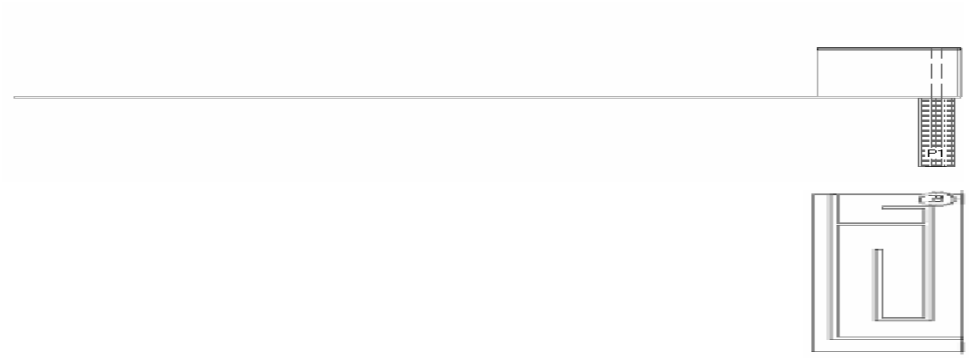

(b)

Figure5.1 Studied Antenna Configuration

As previously seen, the need to use this substrate is to provide mechanical stability of the structure. Contrary to this function, use of the FR4 substrate would have a strong influence on the antenna performance, as it changes the effective dielectric constant under the patch. For example, increasing the thickness of the substrate causes operating frequencies to lower .At the same time increasing the dielectric constant of the substrate

has the same effect. This consequence is observed during the many simulation trials done during the thesis work. The resonant elements forming the whole antenna element have their own shorting pins. Also note that a probe feed at a position close to the shorting point will excite the main radiator. This position for the feeding probe is found (using many trials of simulation) to match the antenna with the characteristic impedance of the coaxial probe used as a feed. The short branch slit is mainly for achieving enhanced impedance matching of the excited resonant frequencies to obtain wider operating bandwidths. The increased impedance bandwidth is expected to be wide enough to cover several operating frequency bands of the mobile communication systems (e.g., GSM900, GSM1800, DCS, PCS, UMTS, etc.).

5.4. Parametric Studies

In this section, the major antenna parameters in relation to the geometry shown in Fig.5.1.will be summarized. Their effects are observed by the simulation package [9].

1) Height of the patch (h): increasing the total height of the patch causes the impedance bandwidth to decrease.
2) Thickness of the substrate material: increasing the substrate material above the air layer causes the operating frequencies to lower. In addition to that, the relative permittivity has similar effect on operating frequencies.

5.5. Results

Figure 5.2 below shows the simulation model of the multiband antenna

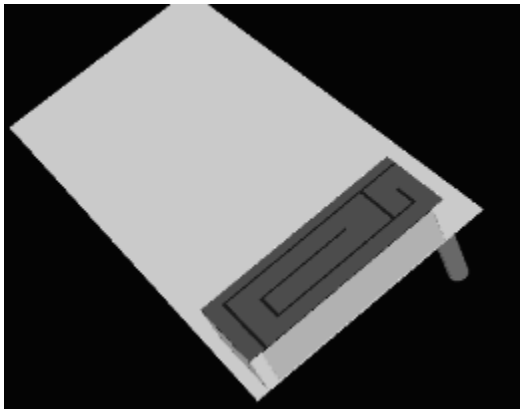

Figure 5.2-Simulation Model of the Multiband Antenna.

In this design, with the PIFA occupying a volume of 13mm x 33mm x 7mm (width x length x thickness) and mounted on top of a ground plane having an area of 40x80mm^2, the obtained impedance bandwidth, determined by 10-dB return loss (or equivalently

2.5:1 VSWR), reaches 556-MHz [that is from 597-1153 MHz] in the lower band, covering the required bandwidth for the GSM 900 band. In the second higher resonating frequency, that is around 1800MHz, taking a return loss below L_{ret} /7.3dB [that is VSWR/2.3]. This band covers the range of frequencies up to 2.2GHz. Therefore, it is clear that the DCS and PCS bands of operations are included in addition to the GSM1800 band. This relatively larger upper band bandwidth is mainly due to the added parasitic shorted patch, which introduces an additional resonant mode to the upper band .Due to this, the upper band become a dual-resonance band. This condition leads to an enhanced impedance bandwidth. In addition, this design has a sufficient bandwidth in the lower band (about 556-MHz) to cover the required bandwidth of the GSM900 operation. In this case, the obtained PIFA design is suitable for applications in GSM900/GSM1800/DCS/PCS quad-band mobile phones. The antenna structure was designed and theoretically studied using the field solver EMPIRE [9].

5.5.1. **Voltage Waveforms at the Input**

As previously done to observe the input impedance, a Guasian pulse voltage of unit amplitude of the form given by equation (5.1) is used. The results of the input impedance are then used to obtain the return loss characteristics of the antenna.

$$V(t) = \exp[-(t-to)/T^2], \qquad (5.1).$$

In Fig.5.3. Below, the voltage amplitudes as a function of both time step and frequency are taken from the simulation. One can observe in Fig5.3 that, the incident and the reflected voltage amplitudes as a function of both time steps (in the final simulation one time step=1.9236e-13seconds) and frequency.

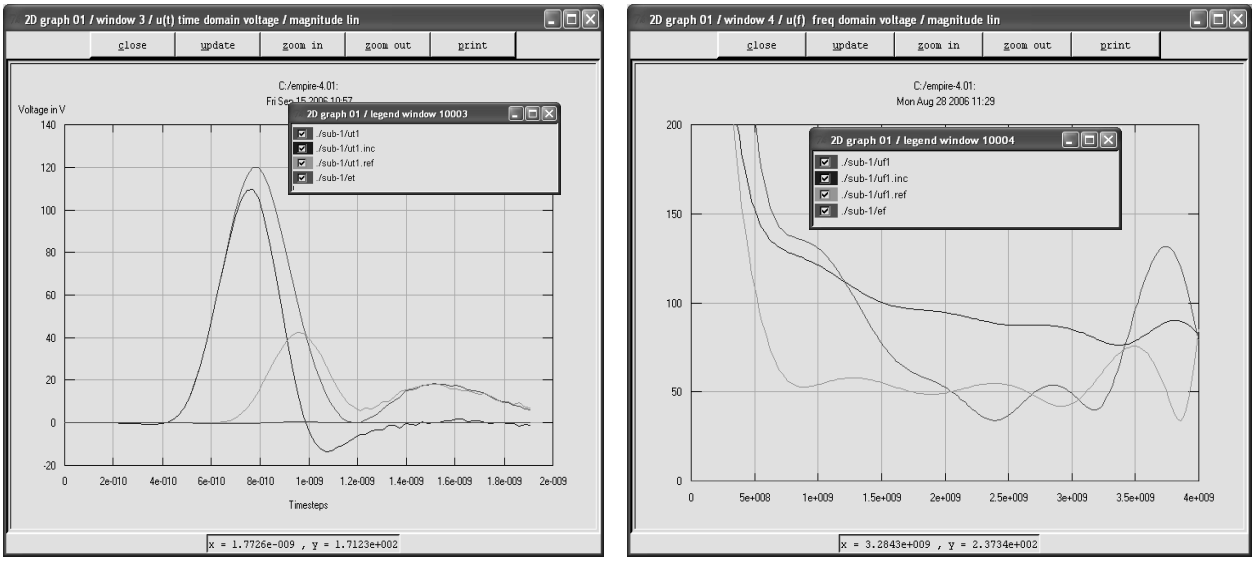

(a) (b)

Figure 5.3 Voltage Waveforms seen at the input terminal of the antenna (a) as a function of time steps (b) as a function of frequency

As can be seen from the snaps above, the reflected voltage amplitude is smaller than that of the incident voltage amplitude, giving a larger return loss for most of the time steps. From the frequency domain voltage, one can also see that the incident voltage is stronger than the reflected giving larger return loss at the expected operating frequencies of the antenna.

5.5.2. Input Impedance

The Figure5.4.below is taken from the simulated output snap that shows the input impedance variation with frequency. As can be seen, one can easily see that around the desired resonant frequencies, the real part of the input impedance attains its maximum and the imaginary part is minimum.

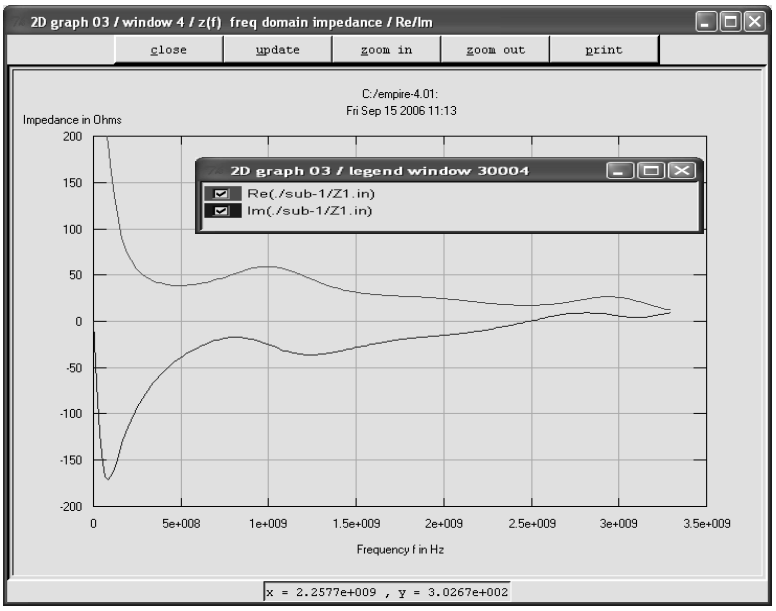

Figure5.4. Input Impedance Plot

5.5.3. Input Return Loss

Based on the design dimensions, the frequency responses of the simulated return loss are shown in Figure 5.5 below. From the simulation results obtained, the first resonant frequency at about 820-MHz is excited with good impedance matching and the second resonant frequency at about 1800MHz is not that much excited strongly and due to this there is a loss of efficiency around this operating frequency.

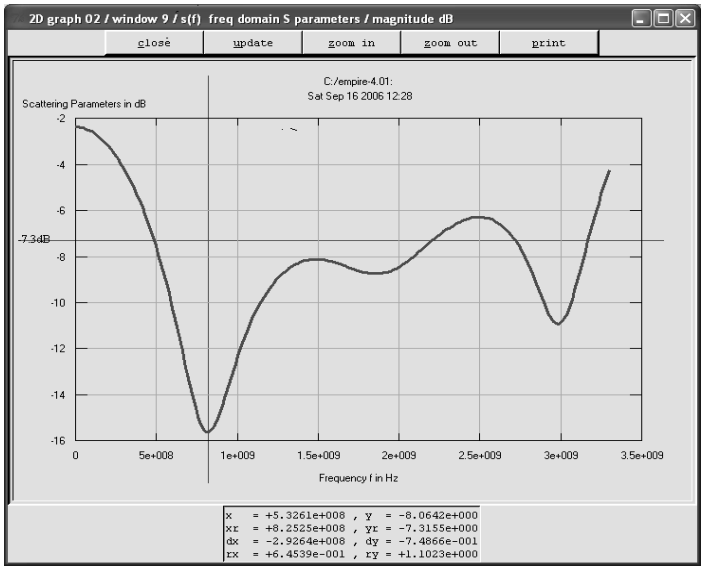

Figure5.5 Return Loss Plot

Another version of the return loss loci on the Smith chart is displayed below as an additional reference for the reader.

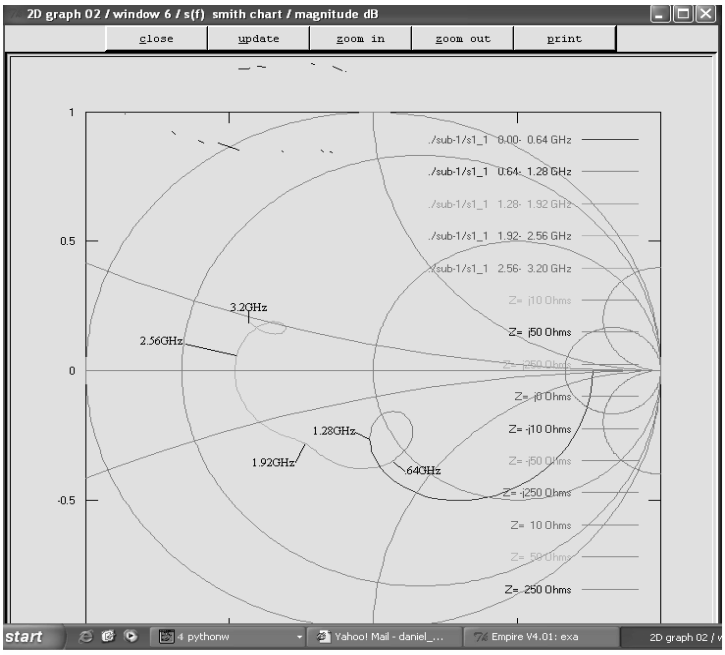

Figure 5.6 Return loss Loci on Smith Chart

From the simulated reflection coefficient curve, the impedance bandwidth (L_{ret}/10-dB) of the lowest band is 67 % of the center frequency f_c=820-MHz.For the dual resonant upper band, the simulated output shows operating region up to 2.2-GHz around the center frequency of f_c=1800-MHz.Above the desired bands there is also a third band with the band width of 450-MHz around the center frequency fc=2.9-GHz.The third band is assumed to be caused by the 3λ/4-resonance of the lower band section of the meandered section. According to the simulation results, the impedance bandwidth of the antenna depends on the length of the ground plane. However, in this design the ground plane length is not optimized with respect to bandwidth. As can be seen, there is a shift in frequency, which is due to the discretization of the structure prior to the simulation.

5.5.4. Radiation Patterns

The simulated cuts of the radiation patterns of the studied antenna are shown in Figure5.7.below. The presented cuts have been obtained in free space. At 900MHz, the radiation pattern is almost omnidirectional and resembles that of a half-wave dipole. Around 1800-MHz, the pattern becomes more complex and somewhat more directive. The directivity increases with frequency. At the same time the pattern maximum tilts

forwards the negative Z-axis. In addition, it can be seen in the figure, that the polarization of the antenna at the lower band is different from the polarization at the upper band.

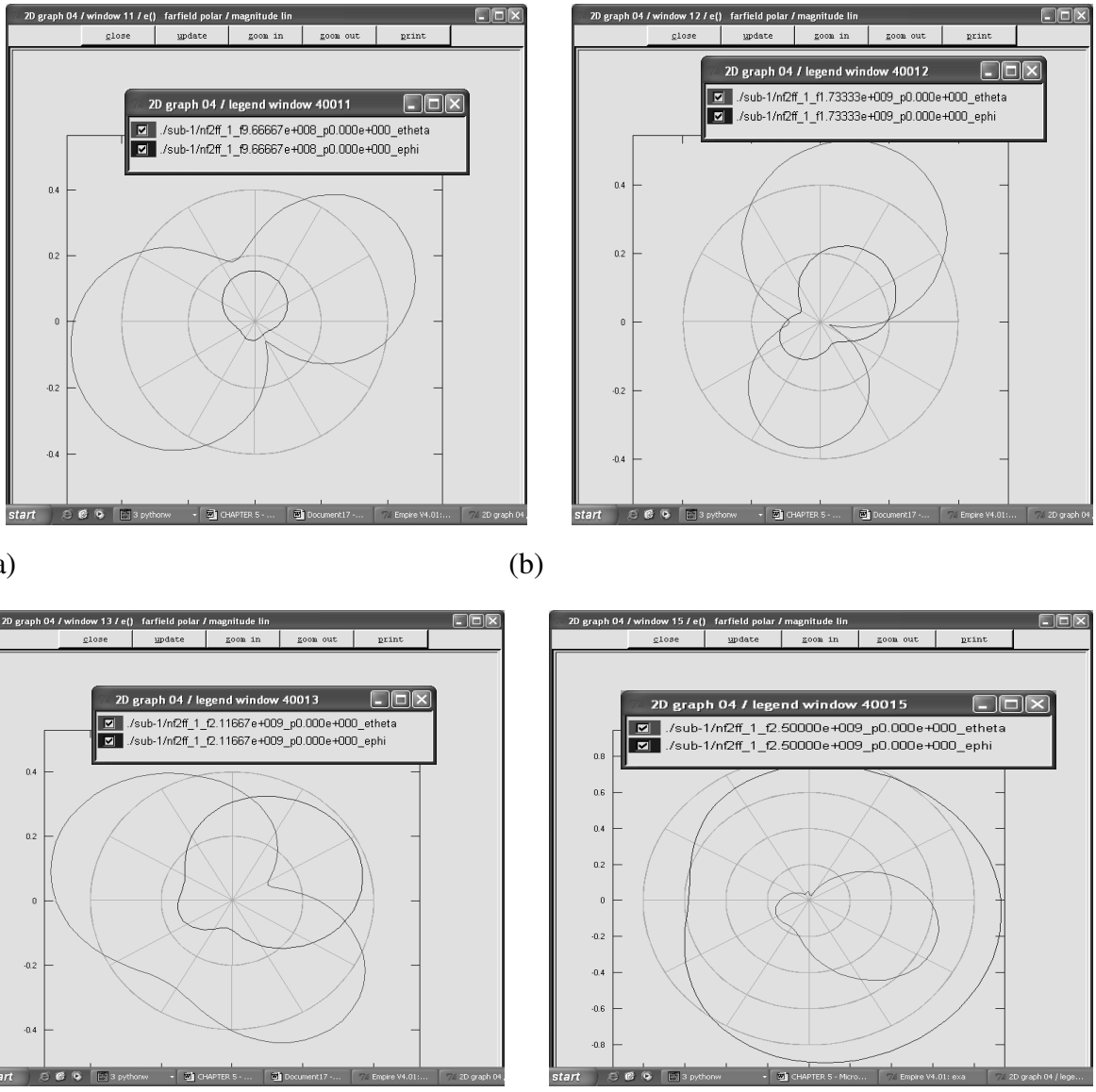

Figure5.7 Radiation pattern both in theta and phi planes (a) around GSM90 (b) around 1800MHz (c) around the DCS band (d) around the UMTS band

The simulated radiation patterns in 3D version of the antenna in each frequency band are displayed in Figure5.8 below .The antenna shows dipole-like behavior for GSM 900,

where as in GSM 1800/PCS frequency bands, the patterns resemble those of typical PIFA antennas. In these bands, the effect of the PCB can also be observed, as a slight deviation of the radiation pattern with respect to the standard patch pattern.

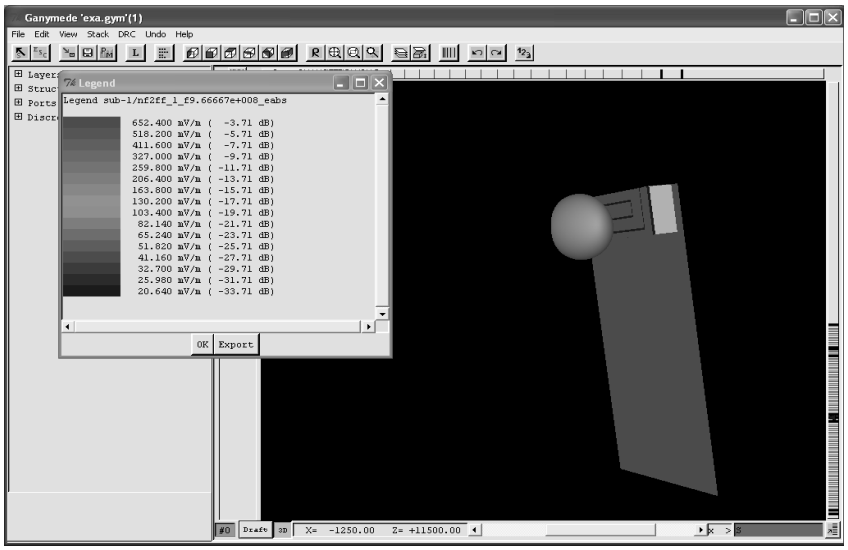

(a) 3D pattern around GSM900

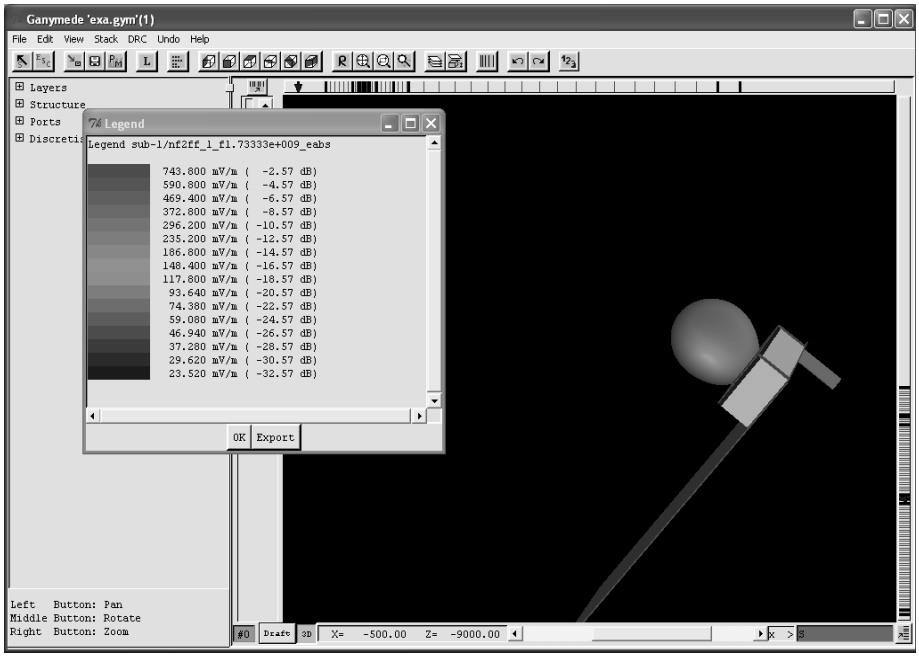

(b) 3D pattern around GSM1800

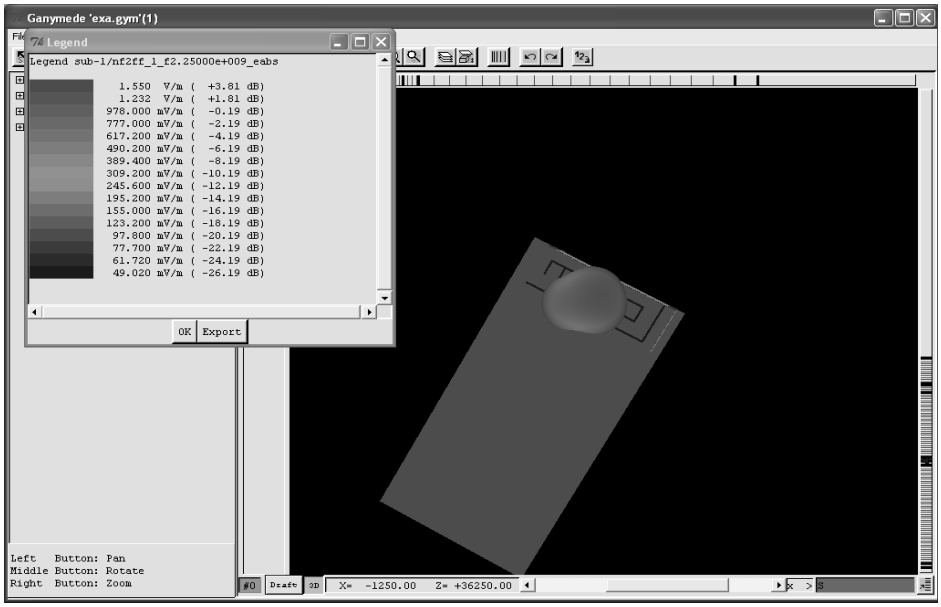

(c) 3D pattern around DCS band.

Figure5.8. Three Dimensional Patterns of the Antenna at different bands

As shown from the simulated outputs we obtain a sufficient bandwidth for the intended multiband operation. But this all is achieved by the small increase in size of the antenna element in order to reserve place for the shorted parasitic patch. Also, before simulation the discretization process approximates some regions and there is some deviation of operating frequencies, which is not that much alarming.

Chapter 6

6.1. Conclusion and Recommendations

In this thesis work single band and multiband antennas have been designed and simulated observations are made on the radiation pattern and input impedance in both cases. From the results of the simulation, it has been observed that the influencing parameters of the antenna are the relative permittivity of the dielectric under the patch, the feed location, the position of the parasitic patch (in the multiband case), and the length and width of the patch.

In the simulation for the single band antenna case there was a problem of some frequency shift fro the intended operating region and this is solved by reducing the thickness of the dielectric material between the patch and the ground plane.
Even though, the software applied for the simulation is efficient, there were problems in long running time and some of the previously done programs must be deleted in order not to disturb the ones at hand.

Compared to previous works on “A monopolar patch antenna with very wide impedance bandwidth” [15], even though the researchers have attained their intended goal, the designed antenna dimension is large compared to the design on this thesis and it is also more complex.

When we see the return loss plots, both antennas have almost a similar response. But the radiation pattern plot of the studied antenna in this thesis work has better directivity and smaller back lobe. Contrary to this, both antennas have stable and monopole-like radiation patterns and are capable of multiband mobile communication systems.

Lastly when we check for the input impedance, the antenna designed by [15] has more or less constant impedance over a range of frequencies. The studied antenna in this thesis has very high input impedance sensitivity to variation in frequency.

In conclusion, this thesis had met the objective of designing and simulating the multiband microstrip patch antenna .It had also provided a sense of achievement as a significant amount of work had been accomplished. However, there are still important areas that require further work and some of them will be illustrated in the next section.

6.2. Recommedation for Future Developments

Although this thesis had provided a significant study on the multiband microstrip antenna system for mobile communications in this era of wireless communications, there are still other equally important areas that require attention.

They include miniaturization of the antenna element with out loss of efficiency, since nowadays the whole apparatus is getting more end more minimized in order to integrate antennas within a minimum space thus requires further research work.

Minimizing electromagnetic energy absorption by the user's head can be another important area of study, since there may be health hazards, if the users head is surrounded by a strong electromagnetic energy for a long time.

Another area of interest is examining the effect of the ground plane dimensions on the performance of the antenna element in order to increase system performance.

APPENDIX A

Derivation of equation 2.37

The derivation of equation (2.37) is taken from page 48 of Stutzman and Thiele (see reference 5). In the ideal case, with no disturbances in the antenna and a perfect match, the input resistance represents antenna dissipation loss. This resistance represents the sum of radiation and ohmic resistances.

$$R_{in} = R_{rad} + R_{loss} \quad \text{(A.1)}$$

Given that the peak current flowing in to the antenna is I_{in}, the average power dissipated is given by equation (A.2):

$$P_{in} = 1/2 \text{ x } R_{in} \text{ x } /I_{in}/^2 \quad \text{(A.2)}$$

Combining equations (A.1) and (A.2):

$$P_{in}=1/2 \text{ x } (R_{in} \text{ x } R_{loss}) \text{ x } /I_{in}/^2$$

$$=1/2 \text{ x } R_{rad} \text{ x } /I_{in}/^2 + ½ \text{ x } R_{loss} \text{ x } /I_{in}/^2$$

Or equivalently:

$$P_{rad}=1/2 \text{ x } R_{rad} \text{ x } /I_{in}/^2 \quad \text{(A.3)}$$

$$P_{loss}=1/2 \text{ x } R_{loss} \text{ x } /I_{in}/^2 \quad \text{(A.4)}$$

The derivation of η (in terms of power), combined with equations ( ) and ( ), Provides the following equation:

$$\eta = \frac{P_{rad}}{P_{in}} = \frac{P_{rad}}{P_{rad} + P_{loss}} = \frac{\left(\frac{1}{2} \times R_{rad} \times |I\,in|^2\right)}{\left(\frac{1}{2} \times R_{rad} \times |I\,in|^2\right) + \left(\frac{1}{2} \times R_{loss} \times |I\,in|^2\right)} \quad \text{(A.5)}$$

Canceling similar terms yields equation (A.6):

$$\eta = \frac{R_{rad}}{R_{rad} + R_{loss}} \quad \text{(A.6)}$$

Appendix B

Brief Review of Finite-Difference Time-Domain (FDTD) Method

1. Introduction

This chapter provides a brief overview of FDTD approximation of partial differential equations. Various important concepts used to benchmark the performance of the FDTD method are introduced. The focus is on linear partial differential equations (PDEs) with one space variable and one time variable. Most of the materials are taken from reference 5.The objective of this appendix is to provide the reader with some background on the mathematical concepts relevant to FDTD method. Therefore detailed mathematical proofs and derivations are omitted as these can be found in the above references.

2. Differentiation and Finite-Difference Operators

The finite-difference method is an approximation to the differentiation operator. Consider function U(x). We could approximate the differentiation $\frac{dU}{dx}$ at x=x_0 with:

$$\frac{d}{dx}U(x_o) \cong \frac{1}{\Delta x}(U(x+x_o)-U(x_o)) \qquad \text{(B.1)}$$

The error associated with this approximation can be determined by using Taylor expansion. Consider the Taylor expansion of a function $f()$ around x :

$$f(x+a) = f(x) + a\frac{d}{dx}f(x) + \frac{a^2}{2!}\frac{d^2}{dx^2}f(x) + \frac{a^3}{3!}\frac{d^3}{dx^3}f(x) + \ldots\ldots\ldots\ldots + \frac{a^{n-1}}{(n-1)!}\frac{d^{n-1}}{dx^{n-1}}f(a) + \frac{a^n}{n!}\frac{d^n}{dx^n}f(\xi)$$

With x[φ[(x+a). Applying this to (2.2.1) and stopping at second order derivative:

$$\frac{1}{\Delta x}(U(x_O+\Delta x)-U(x_O)) = \frac{1}{\Delta x}\left(U(x_O)+\Delta x\frac{d}{dx}U(x_O)+\frac{\Delta x^2}{2}\frac{d^2}{dx^2}U(\xi)-U(x_0)\right)$$

$$= \frac{d}{dx}U(x_0) + \frac{\Delta x}{2}\frac{d^2}{dx^2}U(\xi) = \frac{d}{dx}U(x_0) + O(x_o) \qquad \text{(B.2)}$$

In (B.2) we say that p=O(q) provided $\lim_{p\to 0}(\frac{p}{q})$ exists. Thus the finite-difference error of (B.1) in comparison with actual derivative is proportional to Δx, this error is called the truncation error. Most of the time we are only interested in the values of U (x) at discrete points along the real axis, say $x \in \{x_0, x_1, x_2 \ldots x_{i-1}, x_i \ldots x_m\}$ for a finite interval [a, b]. We may take each x_i to corresponds to:

$X_i = i\,\Delta x$, i= 0,1,2,3…M (B.3)

In general the separation between each set of points does not have to be fixed at Δx.

The corresponding set for U(x) can be defined as:

$U(x) \in \{U_0, U_1, U_2 \ldots U_{i-1}, Ui \ldots U_M\}$

Where $U_i = U(x_i)$. The sets $\{x_0, x_1 \ldots x_{i-1}, x_i \ldots x_m\}$ and $\{U_0, U_1 \ldots Ui_{-1}, Ui \ldots U_M\}$ are known as the grid and grid function. Most cases the scheme of (B.1) at $x=x_i$ can then be written as:

$$\frac{d}{dx}U_i \cong \frac{1}{\Delta x}\left(U_{I+1} - U_i = \delta^+ U_i\right) \qquad \text{(B.4)}$$

The right-hand side of (2.2.4) is known as the forward-difference operator. Table 2.1 shows the various finite-difference operators (Allen and Isaacson, 1998).

$\delta^+ U_i = \frac{1}{\Delta x}(U_{i+1} - U_i)$	Forward-difference
$\delta^- U_i = \frac{1}{\Delta x}(U_i - U_{i-1})$	Backward-difference
$\delta U_i = \frac{1}{\Delta x}(U_{i+1/2} - U_{i-1/2})$	Center-difference
$U_{i+1/2} = \frac{1}{2}(U_{i+1} + U_i)$	Forward-average
$U_{i-1/2} = \frac{1}{2}(U_{i-1} + U_i)$	Backward-average

Table B.1 – Various types of basic finite-difference operators.

The finite-difference operators in Table B.1 are the basic finite-difference operators. From these operators, higher order finite-difference operators, which approximate higher order derivatives can be derived. For instance to approximate $\frac{d^2U}{dx^2}$ at $x=x_i$, we could use the following method:

$$\frac{d^2}{dx^2}U_i \cong \frac{d}{dx}[\delta U_i] \cong \delta(\delta U_i) = \delta\left(\frac{1}{\Delta x}(U_{i+1/2} - U_{i-1/2})\right)$$

$$= \frac{1}{\Delta x}(\delta u_{I+1/2} - \delta U_{i-1/2}) = \frac{1}{\Delta x^2}(U_{i+1} - 2U_i + U_{i-1}) \qquad \text{(B.5a)}$$

Again using Taylor expansion, we could show that the truncation error for (B.5a) is given by:

$$\frac{1}{\Delta x^2}(U_{i+1} - 2U_i + U_{i-1}) = \frac{d^2}{dx^2}U_i + O(\Delta x^2) \qquad \text{(B.5b)}$$

3. Finite-Difference Time –Domain (FDTD) Schemes in One Dimension

Using the finite-difference operators of Table B.1, we could approximate a partial differential equation using an algebra analog. Consider a function in two variables, U(*x,t*) which fulfill the homogeneous hyperbolic partial differential equation (PDE):

$$\frac{\partial U}{\partial t} + a\frac{\partial U}{\partial t} = 0 \qquad \text{(B.6)}$$

In (B.6) we let *t* be the time and *x* be the spatial variable, *a* is a positive real constant. The solution of this PDE is a wave propagating in +*x* direction. First assume *x* is unbounded and *t* is greater than zero. The domain for (B.6) is expressed mathematically as (*x, t*)∈ R^1x{t: t ≥0}, the symbol *x* is called the Cartesian product , while R^1 represents the one-dimensional vector space of real numbers. To get a unique solution, we would need to specify the initial condition, i.e. the values of U (*x, 0*) in (B.6). Such a problem is called the Initial Value Problem (IVP). When the space domain is finite, say (*x, t*)∈ [b, c] x{t: t ≥0}, then additional conditions known as boundary conditions for U (*b, t*) and U(*c, t*) need to be specified to obtain a unique solution. Such a problem is called Initial Boundary Value Problem (IBVP). The issues of existence, uniqueness, the behavior of the solution, and methods to obtain solutions to IVP and IBVP can be found in texts on

partial differential equations. For approximation to the actual solution we are only interested in the function U (*x, t*) at discrete intervals in space and time. Let the discretization be Δx and Δt for space and time, respectively. Also introducing the notation:

$$U_m^n = U(m\Delta x, n\Delta t) \tag{B.7}$$

Where the integer *n* is usually called the time-step in the literature. The basic idea of finite-difference method is to replace the derivatives by finite-difference operators. Since in (B.6) one of the variables is time, the resulting finite-difference operator is called Finite-Difference Time-Domain (FDTD) scheme. Table B.2 shows some FDTD schemes for (B.6). Note that in Table B.2, the subscript for finite-difference operator δ indicates which variable is operated on since U(*x,t*) is now a multi-variable function. For example, δ means forward-difference operator on variable *x*. An important feature of finite-difference method is it approximates a partial differential equation by a set of algebraic equations. This makes it very suitable for application in a computer.

$\delta_t^+ U_m^n + a\,\delta_x^+ U_m^n = 0 \Rightarrow \frac{U_m^{n+1} - U_m^n}{\Delta t} + a\frac{U_{m+1}^n - U_m^n}{\Delta x} = 0$	Forward-time forward-space (B.8a)
$\delta_t^+ U_m^n + a\,\delta_x^- U_m^n = 0 \Rightarrow \frac{U_m^{n+1} - U_m^n}{\Delta t} + a\frac{U_m^n - U_{m-1}^n}{\Delta x} = 0$	Forward-time backward-space (B.8b)
$\delta_t^+ U_m^n + a\,\delta_x U_m^n = 0 \Rightarrow \frac{U_m^{n+1} - U_m^n}{\Delta t} + a\frac{U_{m+1}^n - U_{m-1}^n}{\Delta x} = 0$	Forward-time central-space (B.8c)
$\delta_t U_m^n + a\,\delta_x U_m^n = 0 \Rightarrow \frac{U_m^{n+1} - U_m^n}{2\Delta t} + a\frac{U_{m+1}^n - U_{m-1}^n}{2\Delta x} = 0$	Leapfrog scheme (B.8d)
$\delta_t^+ U_m^n + a\,\delta_x U_m^n = 0 \Rightarrow \frac{U_m^{n+1} - U_m^n}{\Delta t} + a\frac{U_{m+1}^n - U_{m-1}^n}{2\Delta x} = 0$	Lax-Friedrichs scheme (B.8e)

Table B.2- various types of FDTD schemes for one-dimensional hyperbolic partial differential equation.

Each of the scheme (B.8a) to (B.8e) can be written expressing U_m^{n+1} as a linear combination of U_m^n and U_m^{n-1}. By using (B.8a) -(B.8e) with suitable boundary values (U_0^n =f_1(n) and U_M^n =f_2(n) and initial values (U_m^0 ,m=0,1,2,…, M), all subsequent values U_m^n for n=1,2,3,… can be computed directly. Such schemes are known as explicit

as the value of U_m^n at the next instant in time can be found directly from U_m^n of previous time-steps. A simple example serves to illustrate this.

Approach 1: Forward-time forward-space scheme

From (B.8a), we have:

$$U_m^{n+1} = U_m^n - \frac{a\Delta t}{\Delta x}\left(U_{m+1}^n - U_m^n\right) \qquad \text{(B.9.a)}$$

$$U_m^o = g(m\Delta x) \quad \text{and} \quad U_0^n = 0 \qquad \text{(B.9b)}$$

Using conditions of (B.9b), we could determine the values of U_m^n for all non-zero time-steps from (B.9.a). This approach is called single-step scheme as U_m^{n+1} only depends on values of U_m^n.

Approach 2: Leapfrog scheme.

$$U_m^{n+1} = U_m^{n-1} - \frac{a\Delta t}{\Delta x}\left(U_{m+1}^n - U_{m-1}^n\right) \qquad \text{(B.10a)}$$

$$U_m^o = g(m\Delta x) \quad \text{and} \quad U_0^n = 0 \qquad \text{(B.10b)}$$

In the leapfrog scheme, we first use (2.3.4a) to find an estimate for U_m^1 from U_m^0 =g($m\Delta x$). Then this result is used together with U_m^0 in (2.3.5a) to find the values of U_m^n for all subsequent time-steps n=2,3,4…this approach is also called multi-step scheme as U_m^{n+1} depends on values of U_m^n and U_m^{n-1}. Finally at the other end of the domain (x=b), a suitable condition needs to be applied to absorb the positive propagating wave.

4. Characteristics of FDTD Schemes

In analyzing the performance of FDTD schemes, there are various issues to be addressed, such as accuracy of the schemes, consistency, stability, efficiency of the schemes and convergence. In this section the following concepts will be discussed: Convergence, stability, consistency, accuracy.

Definition 1 – Convergence

The error between the actual solution U (x, t) and the numerical solution U_m^n at a certain instance in time is defined as [5]:

$$\varepsilon = \max_m \left| u_m^n - U(m\Delta x, n\Delta t) \right| \qquad \text{(B.11)}$$

A FDTD scheme is convergent if $\in \to 0$ as Δx and $\Delta t \to 0$ for all n.

In general for an accurate scheme, the approximate solution U_m^n must converge rapidly towards the actual solution U (*x, t*) as Δx and Δt approach zero. Also for an FDTD scheme to be stable, the solution for U_m^n must not blow-up as $\Delta t \to 0$ or as *n* is increased to infinity. A more precise definition of stability is given below:

Definition 2- Stability of FDTD Scheme

A one-dimensional FDTD scheme is stable if for any positive time T, there is a constant C_T such that:

$$\left\| U_m^n \right\| \le C \sum_{j=0}^{J} \left\| U_m^j \right\|_T \qquad \text{(B.12)}$$

For $0 \le n\Delta t \le T$

In (B.12) the 'norm' operator $\| \ \|$ is with respect to *m*. Any Euclidean norm will do, for an IVP it is usually taken as:

$$\left\| U_m^n \right\| = \left[\Delta x \sum_m \left(U_m^n \right)^2 \right]^{1/2} \qquad \text{(B.13)}$$

Using the norm allows us to monitor each U_m^n in the set of grid function $\{U_0^n, U_1^n, U_2^n, ..., U_{i-1}^n, U_i^n, ..., U_M^n\}$ (note: M and consequently the set will become an infinite set for an unbounded space). If either U_m^n diverges, (B.13) shows that the norm as a whole also diverges. In a single-step scheme such as Approach 1 of Example 2.1,*J*=0 while for multi-step scheme of Approach 2, *J* =1. Definition 2 tells us that as long as the maximum computation time *T* is finite, C_T will be finite and a constant multiplier of the initial norm will bound the norm at every time-step *n*. The reason why C_T is allowed to be dependent on *T* is that certain solution of the PDE can increase with time. For instance when the homogeneous hyperbolic PDE of (B.6) contains a source, which increases with time, then it is reasonable to assume the solution will increase too. As long as the maximum computation time *T* is finite, the solution should be finite. A powerful method for analyzing stability of linear finite-difference scheme is the Von-Neumann Analysis. This will be used to derive the Courant-Friedrichs-Lewy (CFL) Stability Criterion for Yee's FDTD scheme in Appendix 2.

Another important concept is consistency. In a consistent FDTD scheme, all the finite-difference operators will approach the actual differential operators when the

discretization Δx and Δt approaches zero. For example all the schemes in Table B.2 are consistent.

Definition 3 –Consistency of the Finite-Difference Scheme

Consider a partial differential equation LU= f, where L is the partial differential operator, U (x, t) is the unknown function and f (x, t) the forcing function. If this partial differential equation is approximated by finite-difference scheme $P_{\Delta x,\Delta t} U_m^n = f_m^n$, then the finite-difference scheme is consistent if for any smooth function $\phi(x, t)$:

$$L\phi - P_{\Delta x,\Delta t}\phi \to 0 \text{ as } \Delta x, \Delta t \to 0 \qquad \text{(B.14)}$$

REFERENCES:

1.Constantine A. Balanis, Antenna theory analysis and design, 2nd edition, John Wiley &sons, Inc, 1997.

2.David M.Pozar, Microwave Engineering,3rd edition, Wiley international edition, 2005.

3.Johm D.Kraus,Antennas,2nd edition,McGaraw–Hill Company,1988.

4.Roger F.Harrington,Time Harmonic Electromagnetic Fields, McGraw–Hill Company,1961.

5.Warren L.Stutzman, Gary A.Thiele, Antenna Theory and Design,2nd edition, John Wiley &sons ,Inc,1998.

6.Robert E.Collin, Antennas and Radio Wave Propagation, McGraw-Hill, Inc, 1985.

7.Jean-Francois Zurcher and Fred E.Gardiol, Broadband Patch Antenna, Artech house,Boston,1995.

8.Kin-Lu Wong, Planar Antennas for Wireless Communications, Wiley-interscience,2005.

9.EMPIRE User and Reference Manual, IMST GmbH, 2004.

10. Jay-shong Hong and M.J.Lancaster, Microstrip filters for RF/Microwave applications, Wiley-interscience, 2001.

11.JR James and PS Hall, Handbook of Microstrip Antennas, Vol. 1&2,Pete Peregrinus Ltd

12. Sophocles J. Orfanidis, Electromagnetic Waves and Antennas, ECE department, Rutgers University, 2004.

13.Y.T.Lo and S.W.Lee, Antenna Handbook Theory, Application and Design, Van Nostrand Renhold Company, New York, 1988.

14. Shiban K. Koul, Millimeter Wave and Optical Dielectric Integrated Guides and Circuits, John Wiley and Sons, INC, 1997.

15.K.-L.Lau**,** P.Li, K. -M.Luk, "A Monopolar Patch Antenna With Very Wide Impedance Bandwidth ", IEEE TRANSACTION ON ANTENNAS AND PROPAGATION, VOL.53, NO.2, FEBRUARY 2005,PP655-661.

16. Shimels Mamo,"Analysis and Design of Dual band Microstrip Antennas for Mobile Handsets ", Master's thesis, Unpublished, 2005.

Declaration

I, the undersigned, declare that this thesis is my original work, has not been presented for a degree in this or any other university, and all sources of materials used for the thesis have been fully acknowledged.

Name: Daniel Mammo

Signature: _____

Place: Addis Ababa

Date of submission: _____

This thesis has been submitted for examination with my approval as a university advisor.

Dr.Ing. Mohammed Abdo _____

Advisor's Name Signature